Li, Fang; Suominen, Mikko; Lu, Liangliang; Kujala, Pentti; Taylor, Rocky

A probabilistic method for long-term estimation of ice loads on ship hull

Published in:
STRUCTURAL SAFETY

DOI:
10.1016/j.strusafe.2021.102130

Published: 01/11/2021

Structural Safety 93 (2021) 102130

Contents lists available at ScienceDirect

Structural Safety

journal homepage: www.elsevier.com/locate/strusafe

A probabilistic method for long-term estimation of ice loads on ship hull

Fang Li [a,*], Mikko Suominen [a], Liangliang Lu [a], Pentti Kujala [a], Rocky Taylor [b]

[a] Aalto University, School of Engineering, Finland
[b] Memorial University of Newfoundland, Faculty of Engineering and Applied Science, Canada

ARTICLE INFO

Keywords:
Ice load
Long-term estimation
Probabilistic method
Event Maximum Method
Full-scale measurement
Ice-going ships

ABSTRACT

Ships navigating in ice-infested regions need strengthened hull to resist the loads arising from the interactions with ice. Correct estimation of the maximum ice loads a ship may encounter during its lifetime is of vital importance for the design of ship structures. Due to the stochastic nature of ice properties and interaction processes, probabilistic approaches are useful to make long-term estimations of local ice loads on the hull. The Event Maximum Method (EMM) is an existing probabilistic approach for the long-term estimation of ice loads on the hull. This paper aims to extend the current EMM, first by introducing a model for the intercept of the linear regression line on the abscissa in order to quantify this value. Moreover, ice concentration is considered in the extended method as the second ice condition parameter in addition to thickness. The proposed method is applied to the full-scale measurement of the ship S.A. Agulhas II using the data obtained from the 2018/19 Antarctic voyage. The obtained model is then validated against six-year measurement data from 2013 to 2019, which shows reasonable similarity.

1. Introduction

Ships sailing in ice-covered water are subject to considerable contact with ice. To prevent ship hull from major damage during its lifetime, the maximum ice load exerted on the hull needs to be estimated to set up the classification rules and to design the local structure. The maximum ice load can be estimated by theoretical methods via first-principle approaches, e.g. [1,2], or empirical methods via probabilistic approaches, e.g. [3–7]. Due to the complexity of ice failure, and the inherent challenges associated with the development of physics-based ice mechanics models over the wide ranges of scales needed to capture representative continuum and discrete ice failure processes, theoretical methods have to be based on a considerable number of assumptions in terms of ice material behaviour. Empirical methods have the advantage that the models are based on measurement, where physical processes are reflected correctly with all natural variations present. The random nature of ice properties and ship-ice interaction processes also makes probabilistic approaches suitable to capture the stochastic behaviour of local ice loads.

Ideally, one would expect a model to link the prevailing ice conditions to the ice load distribution parameters, so that the long-term extreme loads can be estimated based on the ice condition a ship may encounter during its lifetime. However, such modelling attempts are very rare in the literature. Kujala [3] presented the first such model linking ice thickness to the Gumbel distribution parameters of 12-hour maximum ice loads. Kotilainen et al. [4] later adopted hierarchical Bayesian modelling to link ice thickness and ship speed to short-term ice load distributions. More recent work was carried out by Shamaei et al. [8], in which the Event Maximum Method (EMM) was applied to link ice thickness to the distribution parameters of measured ten-minute maxima. This paper further extends the work of Shamaei et al. [8].

EMM was initially proposed by Jordaan et al. [9] for the estimation of long-term extreme ice pressure due to ships ramming in ice. This method adopts linear regression to the tail of ice pressure measured by pressure panels plotted versus the corresponding negative logarithm of the probability of exceedance. The regression line is characterized by two fitting parameters, including α denoting the reciprocal of the slope and x_0 the intercept on the abscissa. Differentα and x_0 are obtained for different areas (denoted by A) under consideration. Jordaan et al. [9] then fit the α-area relationship by $\alpha = CA^{-D}$. To apply the method, x_0 is assumed to be zero or a chosen value and α is calculated based on the design area. The maximum ice pressure corresponding to a given return period can then be calculated. This method has been later applied and extended for the estimation of long-term ice pressure by Taylor et al. [10], Li et al. [11], Brown et al. [12], Ralph [13] and Rahman et al. [14]. Shamaei et al. [8] applied the same methodology to the ice force data

* Corresponding author.
E-mail address: fang.li@aalto.fi (F. Li).

https://doi.org/10.1016/j.strusafe.2021.102130
Received 22 December 2020; Received in revised form 23 April 2021; Accepted 5 July 2021
Available online 21 July 2021

during continuous navigation measured by strain gauges instrumented on frames. The method is slightly modified to use ice thickness instead of design area as the explanatory variable to define α-thickness curves. Their work shows that EMM can be as well applied to ice force data measured on a frame conditionally on visually observed ice thickness.

While in design practice, x_0 has often been assumed to be zero in applications of EMM, as pointed out by Taylor et al. [10] and Li et al. [11], this may be a conservative assumption when the areas under consideration are small. As discussed in ISO-19906 (2019) [15], designers may choose alternative values based on analysis of appropriate regional local pressure data when available. For the ice load on one ship frame with frame spacing around 0.5 m, the contact area is typically small (mostly < 1 m^2). As will be shown in this paper, the assumption of x_0 equaling zero is not representative and is not always conservative for our dataset. In order to apply EMM for such cases, a model of x_0 is necessary. Therefore, the first aim of this paper is to develop a method to model x_0 so that EMM can be used to estimate the long-term ice force on one or several ship frames.

In addition to ice thickness, another factor significantly influencing ice load magnitude during ship operation is ice concentration. Ice concentration is not relevant for ships ramming thick ice since exposure is treated by modelling the number of impact events, which is the case of Jordaan et al. [9]. However, it is highly relevant when continuous operation is involved since it is expected that ships in higher ice concentrations will have more ice impacts and therefore higher exposure. This is particularly important when data are recorded as 10-minute maxima rather than being analyzed as a series of impacts with different event duration. Shamaei et al. [8] did not account for ice concentration in their application of EMM. The second aim of this paper is then to extend EMM to include ice concentration as an additional ice condition variable. In this way, the estimation of long-term maxima can be dependent on both ice thickness and concentration, which leads to generalization of the results based on commonly reported sea ice conditions.

The data used in this paper are obtained from the ship S.A. Agulhas II during its Antarctic voyages. Unlike the previous applications of EMM where pressures are measured, the line loads are measured and used in this paper. For this reason, the notation α in previous EMM applications is replaced by β to make the distinction. The data are gathered from six voyages spanning from 2013/14 to 2018/19. The extensive data across multiple years make it possible not only to establish a model based on the data, but also to validate the model with longer-term measurements, which is rare in the literature. In this paper, the data obtained from the 2018/19 voyage are used to build a model following the proposed method; the six-year data are then used to validate the model. This provides new insights into the validity of the proposed method for the estimation of long-term extreme loads.

2. Event maximum method

Jordaan et al. [9] proposed the Event Maximum Method for the estimation of ice pressure based on the measurement through pressure panels. A pressure panel consists of a number of subpanels with known area, each giving a pressure measurement during a ramming event. For each ramming event, the maximum pressures recorded by the individual subpanels are extracted and later used for statistical analysis. The value of the maximum pressure is denoted here by the sequence $(X_1, X_2, \cdots, X_n)$, where n is the total number of ramming events and the subscripts are the indices of the ramming events. The sequence of X is then ranked by their magnitude, resulting in a new sequence $(X_{(1)}, X_{(2)}, \cdots, X_{(n)})$ in descending

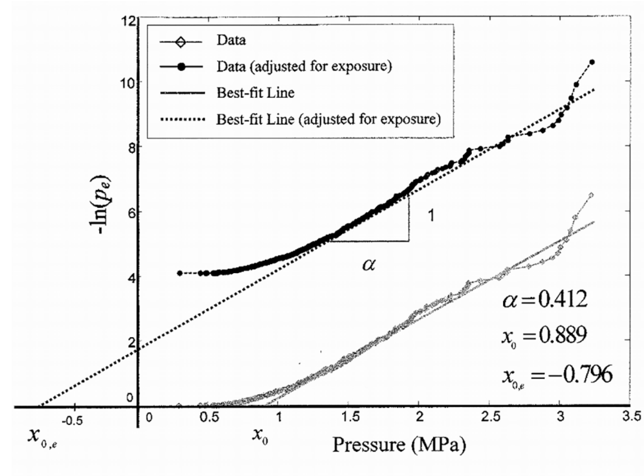

Fig. 1. Illustration of the local pressure methodology for sample event [10].

order. The probability of exceedance is then defined based on the empirical cumulative distribution using Weibull plotting position:

$$p_e(X_{(i)}) = \frac{i}{n+1} \tag{1}$$

$X_{(i)}$ is then plotted on the exponential probability paper, i.e. plotted against the negative natural logarithm of p_e, illustrated in Fig. 1. It was observed that the tail of the scatter plot is approximately linear, indicating that the tail can be fit with an exponential distribution, which has its probability of exceedance in the following form:

$$-\log(p_e(x)) = \frac{x - x_0}{\alpha} \tag{2}$$

Through a linear regression to the scatter plot, x_0 and α can be obtained. Since each maximum pressure $X_{(i)}$ is the maximum of an array of pressure values measured by m subpanels, if the focus is on a specific subpanel area, the denominator of the right side of Eq. (1) should be replaced by $mn + 1$. This is equivalent to shifting the scatter plot upwards, which does not change α but results in a different x_0 ($x_{0,e}$ in Fig. 1). Different α values can be obtained for different areas under consideration. Jordaan et al. [9] then fit the α-area relationship by the following function

$$\alpha = CA^{-D} \tag{3}$$

where C and D are parameters to be obtained from the regression.

To apply the method, the maximum pressure Z of N ramming events which hits the pressure panel is of concern, i.e.

$$Z = \max(X_1, X_2, \cdots X_N) \tag{4}$$

Fig. 2 illustrates the relationship between the probability density function (PDF) of X and Z. The cumulative distribution function (CDF) of Z can be derived based on the CDF of X by

$$F_Z(z) = F_X(z)^N = \left(1 - \exp\left(-\frac{(z - x_0)}{\alpha}\right)\right)^N \tag{5}$$

When N is large, Eq. (5) is asymptotic to the Gumbel distribution

$$F_Z(z) = \exp\left(-\exp\left(-\frac{z - x_0 - x_1}{\alpha}\right)\right) \tag{6}$$

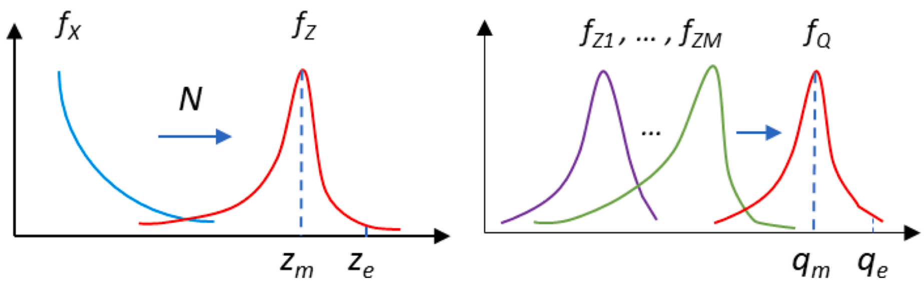

Fig. 2. Illustration of the derivation from the PDF of X to Z and then to Q, left: derivation of the PDF of long-term maxima based on the PDF of event maxima within the same category, presented in Eqs. (4)–(9); right: derivation of the PDF of long-term maxima across different categories based on the PDF of long-term maxima within the same category, presented in Eq. (9)–(12).

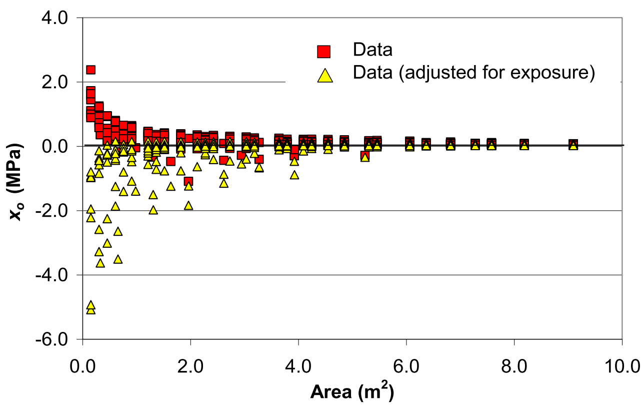

Fig. 3. Plot of x_0 data showing results both with and without adjustment for exposure effects [10].

where $x_1 = \alpha \log N$. The characteristic extreme value corresponding to the return period of N is then

$$z_m = x_0 + x_1 = x_0 + \alpha logN \quad (7)$$

In practice, to ensure safety, the value z_e corresponding to a probability of exceedance of p_e is often of interest. z_e can be obtained by equaling Eq. (6) to 1 $-p_e$, resulting in the following expression

$$z_e = x_0 + \alpha[-\log(-\log(1-p_e)) + \log N] \quad (8)$$

Jordaan et al. [9] assumes x_0 as zero, so the value of z_e in Eqs. (7) and (8) is determined by α and N. Taylor et al. [10] highlighted that x_0 varies as a function of interaction area (see Fig. 3) and discussed the importance of accounting for effects of exposure on x_0. The readers are referred to Jordaan et al. [9] and Taylor et al. [10] for more details and examples of this method.

Shamaei et al. [8] adopted the same methodology for continuous navigation in ice but used a different definition for an *event*. Table 1 summarized the differences between Shamaei et al. [8], Taylor et al. [10] and Jordaan et al. [9]. In the application of Jordaan et al. [9], an *event* is defined as a ship ram, and a *maximum* is defined as the maximum pressure among the subpanels during a whole ramming process. A similar definition was used by Taylor et al. [10], except that individual loading *events* were extracted from datasets for continuous operations in sea ice, as well as from discrete ramming events for datasets involving multi-year ridge and glacial ice impacts. Such definitions allow the analysis of pressure conditionally on a given panel area for ramming events. In the work of Shamaei et al. [8], the method is applied to data mainly including ship continuous operation. An *event* is then defined as a ten-minute operational period. The selection of ten-minute as the duration of each event is due to a practical reason that the visual observations of the ice condition are summarized for each ten minutes. A *maximum* is then defined as the maximum pressure on a frame during a ten-minute period, i.e. during an event. In this case, there is no need for exposure adjustment (see Fig. 1) because there is no similar distinction to that between a panel and subpanels. The focus is on ten-minute maxima, so the number of ice load peaks and the magnitude of the individual load peaks within each ten minutes (i.e. an *event*) are irrelevant. Within each ten-minute interval, the maximum ice pressure is linked to the maximum ice thickness observed during this period. In other words, it is assumed that the maximum ice thickness causes the greatest load. Because of this, it is convenient to use ice thickness instead of area as the variable influencing x_0 and α. Shamaei et al. [8] then followed the Jordaan et al. [9] procedure to get several α-thickness curves for the frames on the bow, bow shoulder and stern shoulder regions of the S.A. Agulhas II. Examples of the curves are given in Fig. 4.

To apply the results, one need to define the operational time a ship navigates in different thickness categories, and divide the operational time in minutes by ten minutes to calculate the number of ten-minutes sections as the exposure to each thickness category, i.e. the N in Eq.

Table 1
Comparison of Jordaan et al. [9], Taylor et al. [10] and Shamaei et al. [8].

	Jordaan et al. [9]	Taylor et al. [10]	Shamaei et al. [8]
Event	Ship ice ramming process	Discrete ship ice loading events from continuous navigation	Ten-minute operational intervals in ice during continuous navigation
Maximum	Maximum pressure among the subpanels during a ram	Maximum pressure among the subpanels during each event	Maximum (estimated) pressure within each ten-minute period
Explanatory variable	A defined area	A defined area	Maximum ice thickness for fixed frame width

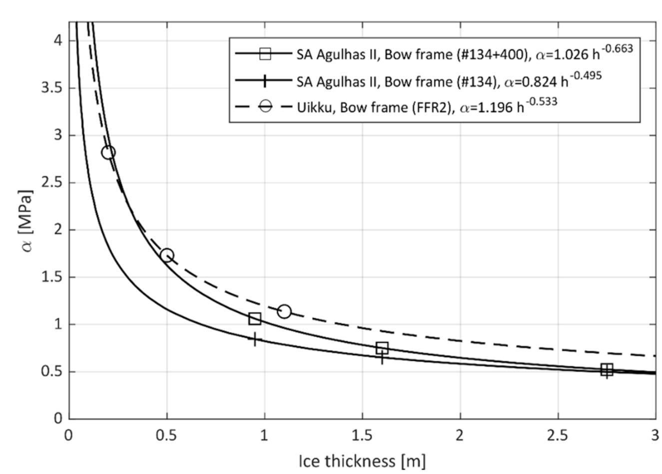

Fig. 4. Some α-thickness curves obtained by Shamaei et al. [8].

(8). Examples will be given later in Section 6. This differs from Jordaan et al. [9] where N is the number of ramming times.

In the dataset of Shamaei et al. [8], the pressure is not directly measured; it is estimated from the measured ice force with an assumption that the contact height equals 0.3 times ice thickness. We could equivalently focus on the line load instead of the pressure so that the assumption of contact height is not needed; this approach will be followed in this paper.

There is one more difference in the application of the results, although not explicitly mentioned by Shamaei et al. [8]. With Jordaan et al. [9], α is calculated from an area on the hull, thus is independent of ice parameters. However, with Shamaei et al. [8], α values are calculated corresponding to the estimated prevailing ice thicknesses.. Therefore, for the same ship frame, there can be different α values corresponding to different ice thickness categories. Then based on the exposure of a ship in different ice thickness categories, one can estimate different extremes corresponding to each ice thickness category via Eq. (6). If these extremes are denoted by Z_i,where $i = 1, 2, \cdots, M$ and M is the index of ice thickness categories of concern, each Z_i then has the distribution described by Eq. (6) with the exposure N substituted byN_i. The interest is the maximum ice load encountered during navigation in all ice thickness categories, which is

$$Q = \max(Z_1, Z_2, \cdots Z_M) \tag{9}$$

The relationship between the PDF of Z and Q is presented in Fig. 2. Similar to Eq. (5), the cumulative distribution function of Q is

$$F_Q(q) = \prod_{i=1}^{M} F_{Z_i}(q) = \prod_{i=1}^{M} \exp\left(-\exp\left(-\frac{q - x_{0,i} - x_{1,i}}{\alpha_i}\right)\right) \tag{10}$$

where $x_{1,i} = \alpha_i \log N_i$. It is not straightforward to find the inverse function of Eq. (10) analytically to get solutions similar to Eqs. (7) and (8). But this can be easily evaluated numerically. One can find the most probable extreme value q_m numerically with Eq. (10) by searching for the value of q which maximize $\frac{dF_Q(q)}{dq}$, i.e.

$$q_m = \underset{q}{\operatorname{argmax}} \frac{dF_Q(q)}{dq} \tag{11}$$

One can then find the q_e corresponding to a probability of exceedance p_e by numerically solving

$$F_Q(q_e) = 1 - p_e \tag{12}$$

3. Dataset

3.1. Description of the dataset

A brief description of the full-scale measurement which provides the dataset used in this paper is given here. The Polar Supply and Research Vessel (PSRV) S.A. Agulhas II is instrumented with shear strain gauges on a total of nine frames at the starboard of the ship. These includes two at the bow, three at the bow shoulder and four at the stern shoulder (see Fig. 5). The shear strains are measured and then converted to forces on each frame according to Suominen et al. [16]. The forces are recorded at a frequency of 200 Hz. The data in focus here is the measurement at the bow region.

Ice conditions including ice thickness, concentration, floe size and ridge information have been recorded by visual observations through all the Antarctic voyages (see [1718] for more information). Visual observations are conducted at the bridge of the ship, with a reference measurement stick to estimate the ice thickness and visual estimation to estimate ice concentration. The visual observation is conducted approximately once in a minute and then summarized for each ten-minute period. The ice thickness and concentration used in this paper are the maximum observed values within each ten minutes.

The ship has been travelling to Antarctic every austral summer from 2012/13 to 2018/19. In this paper, the data of 2018/19 voyage is used for establishing the model and the data from 2013/14 to 2018/19 are used for the validation of the model. The 2012/13 voyage is excluded because the visual observations were summarized every 15 min, which deviates from other voyages. The 2018/19 voyage dataset is chosen for

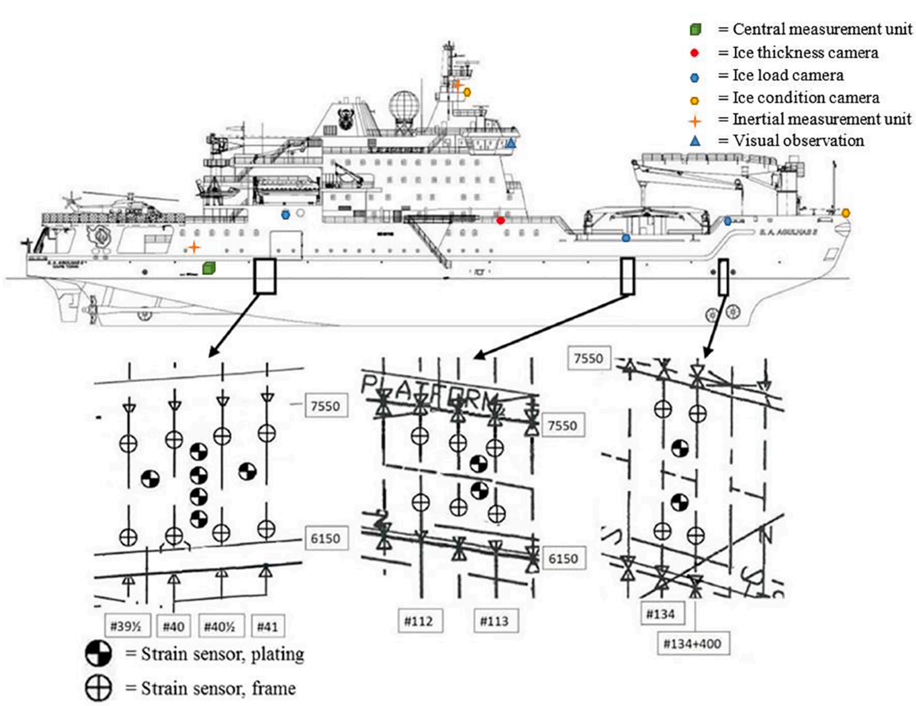

Fig. 5. Instrumentation of S.A. Agulhas II.

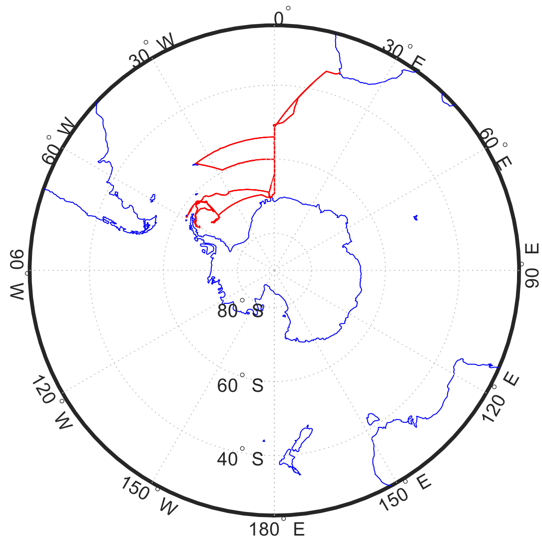

Fig. 6. Route of the 2018/19 Antarctic voyage.

modelling because (1) the number of ice loads the ship encounters is large, and (2) it covers wide ranges of thickness and concentration. In addition, ice condition cameras have been installed during this voyage, which in future may provide higher-resolution ice condition data through machine vision [19], thereby improving model quality. Besides, the 2014/15 voyage dataset also meets the above two criteria but with no ice condition camera for later calibration. The 2014/15 voyage dataset is then selected as an alternative training dataset to investigate the yearly variation of the obtained model. Fig. 6 illustrates the route of the ship in the 2018/19 voyage. The ship departed from Cape Town, South Africa, on 6 December, heading towards Penguin Bukta located on the Antarctic ice shelf; then visited Weddell Sea and finally returned to Cape Town on 15 March. The route of the ship during other voyages are similar to the 2018/19 except for the travel to the Weddell Sea. The results obtained in this paper are regarded suitable for the estimation of long-term ice loads for ships navigating through similar areas in the Antarctic summer season. The readers are referred to Kujala et al. [20] for a summary of ice thickness and ice loads encountered in each year, and references [2122] for more information about the 2018/19 voyage.

3.2. Categorization of the dataset

In the 2018/19 Antarctic voyage, there are in total 1093 *events* from the visual observation record, each containing a ten-minutes period with ice presence. Following the methodology of Jordaan et al. [9], regression analysis is to be conducted on the data with the same explanatory variables, which are the ice thickness and concentration in this paper. These 1093 events then need to be divided based on the maximum thicknesses and concentrations into different categories. The total number of categories is then the product of the number of thickness categories and concentration categories. To ensure enough data falling into most categories, the following categorization in Table 2 is adopted in this paper.

Here c denotes concentration and h denotes thickness. In the following text, a category is referred to by combining the concentration and thickness category names, e.g. C1H1. The two concentration categories divided by 80% roughly correspond to ice fields where ships can avoid major collisions with ice via maneuvering and ice fields where collisions can hardly be avoided. Since visual observations inevitably contains uncertainties, such grouping of data into categories with relatively wide intervals reduces the rate of misclassification of the ice force data.

The notation α has commonly been used to represent pressure with unit of Pa or MPa. Since this paper employ line load data instead of pressure data, another symbol, β, is used to represent the line load with unit of kN/m, so as to be distinguished with cases where EMM is applied to pressure data. The difference is merely the notation; the theory remains the same.

3.3. Dataset on exponential probability paper

Before presenting the extended EMM in the next Section, we will first investigate whether x_0 equaling zero is a valid assumption with the S.A. Agulhas II dataset. To demonstrate this, linear regressions are conducted separately to the line load data of each category plotted versus the corresponding negative $\log p_e$. Here the ‘tail’ is set as the upper 20% of the data in each category; the dataset of frame #134.5 is used here as an example. Fig. 7 shows the regressions and Fig. 8 summarizes the β and x_0. At the current step, we aim to find the overall trend of β and x_0 in order to assist reasoning, instead of focusing on the specific values obtained from the regressions.

Some observations regarding x_0 from Fig. 8 are:

- The magnitude of x_0 can be up to 40% of the measured maximum line loads, e.g. in C1H1, C1H3, C2H5. According to Eqs. (7) and (8), the long-term extremes are calculated as the summation of x_0 and another term. The assumption that x_0 is a constant does not reflect the data and a value $x_0 = 0$ is not appropriate for this case.
- The magnitude of x_0 seems to be larger with high concentration, except for the categories with h > 200 cm. This is reasonable because high concentration corresponds to more load peaks within each ten-minute, therefore resulting in higher ten-minutes maxima.
- With thickness increasing, the magnitude of x_0 first increases and then decreases.

The above first point indicates clearly that x_0 should not be assumed to be zero for the line load dataset. The latter two points help to find out a proper way to model x_0. This will be presented in Section 4.

4. A proposed method based on EMM

4.1. Assumptions

The fundamental assumptions behind the method to be proposed include:

- Assumption 1: The ten-minute load maxima under the same ice condition (here thickness and concentration) are independently and identically distributed.
- Assumption 2: The distribution of ten-minute load maxima has exponential distribution tail, similarly to Fig. 1.

Assumption 1 is the fundament of methods and investigations based on fixed-interval maxima. The independence can be justified by that what a ship meets in a ten-minute period is independent of other periods. The identity, however, does not rigorously hold. Ice load is known

Table 2
Number of events falling into each category.

	H1 (h<=40 cm)	H2 (40 cm < h<=80 cm)	H3 (80 < h≤120 cm)	H4 (120 cm < h<=200 cm)	H5 *(200 cm* < h<=300 cm)
C1 (c<=80%)	77	122	94	52	13
C2 (c > 80%)	22	235	240	107	57

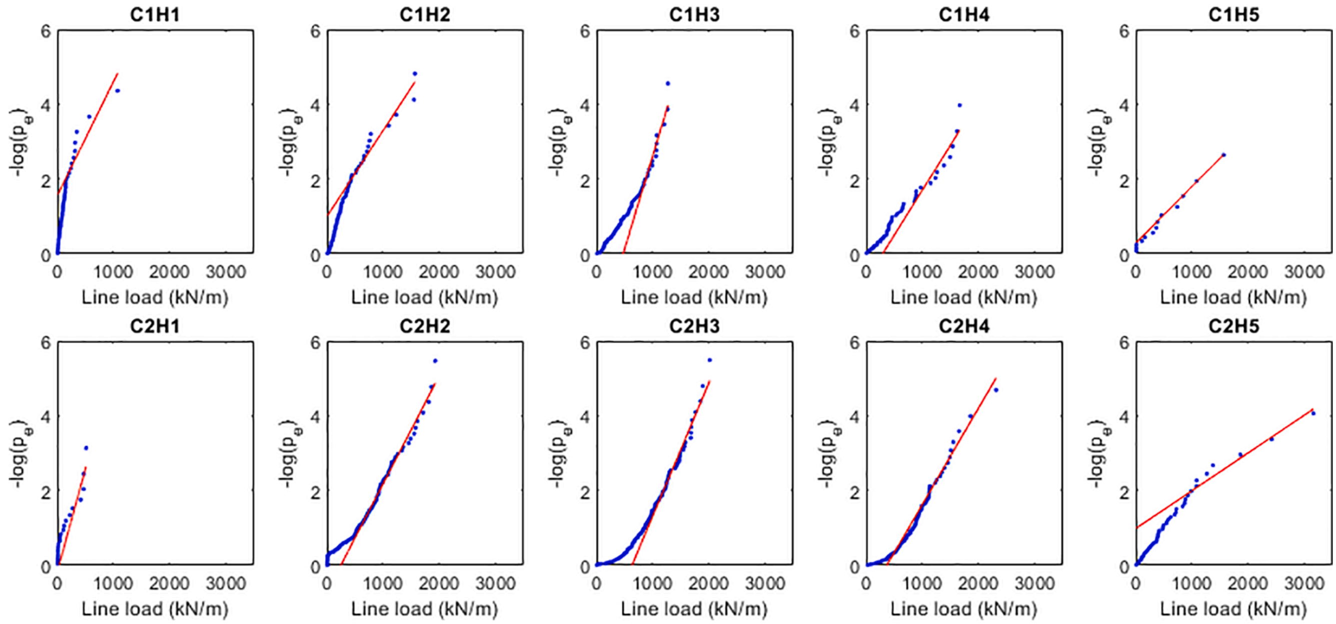

Fig. 7. Linear regression to the tail of the data in each category.

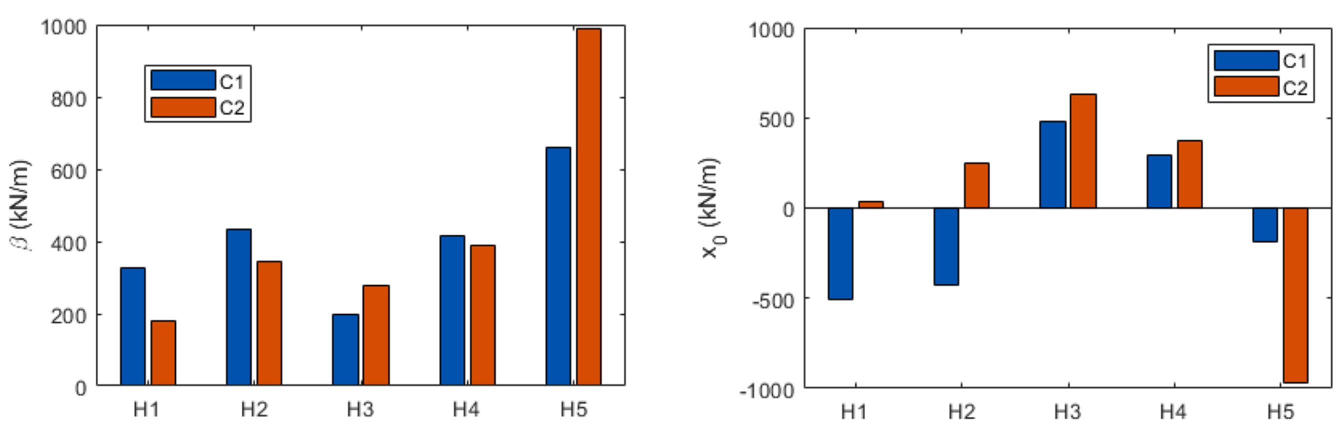

Fig. 8. Fitted β and x_0

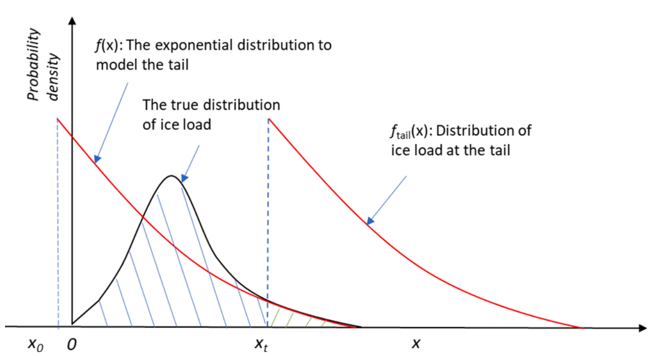

Fig. 9. Illustration of exponential fitting to the tail with probability density function.

to be influenced by ship operation such as speed and maneuvering in addition to ice condition. Therefore, the correctness of identity is conditional on that the maneuvering behavior and speed control of the ship does not change for different ten-minute periods with the same ice condition. Since the data used here are obtained under normal operation, i.e. the crew maneuver the ship through ice and control the speed according to the operational profile of the ship, the identify can be assumed to hold in a rough order.

Assumption 2 arises from the fundament of Event-Maximum Method following Jordaan et al. [9]. This assumption comes from visual examination of the load data plotted on exponential probability paper, which shows that the upper tail looks linear, thus featuring exponential tail. This then involves the definition of 'tail' to quantify how much data fall into there. It has been shown by Shamaei et al. [8] that for the ten-minute-maxima dataset of line loads, it can be reasonably assumed that the upper 20% of data represent the 'tail'. This is reflected in Fig. 9, where x_t is the load value at the 80% percentile. The probability mass of the load distribution is then 0.8 in the region of $x < x_t$, and 0.2 in the region of $x \geq x_t$. This will be followed here.

4.2. Re-formulation of EMM

The original EMM adopts probability paper (Fig. 1) for the estimation of distribution parameters. Here the method is re-formulated to also enable maximum likelihood estimation and uncertainty analysis. EMM essentially seeks the exponential distribution whose tail can properly describe the tail of the load distribution, see Fig. 9. This exponential distribution is characterized by x_0 and β, expressed by

$$f(x) = \frac{1}{\beta}\exp\left(-\frac{x-x_0}{\beta}\right) \tag{13}$$

Given that a load value $\times$ is located in the tail (i.e. $x \geq x_t$), its probability density function can be derived by

$$f_{tail}(x) = f(x|x \geq x_t) = \frac{f(x)}{1-F(x_t)} = \frac{\frac{1}{\beta}\exp\left(-\frac{x-x_0}{\beta}\right)}{\exp\left(-\frac{x_t-x_0}{\beta}\right)} = \frac{1}{\beta}\exp\left(-\frac{x-x_t}{\beta}\right) \tag{14}$$

which is simply another exponential distribution with the same β but bounded at x_t (see Fig. 9). Since x_t is the 80% percentile of $f(x)$, x_0 and x_t are linked by

$$x_0 = x_t - \beta(-\log(1-0.8)) = x_t + \beta\log(0.2) \tag{15}$$

The aim is to find the relationship between distribution parameters (x_0 and β) and ice condition variables (here thickness h and concentration c), expressed as

$$\beta = f_\beta(h,c) \tag{16}$$

$$x_0 = f_{x_0}(h,c) \tag{17}$$

With Eq. (15), we have

$$x_t = f_{x_t}(h,c) = f_{x_0}(h,c) - \beta\log(0.2) \tag{18}$$

There are two equivalent options to model x_0 and β. The first is to model x_0 directly by finding $f_{x_0}(h,c)$, while the second is to model x_t by finding $f_{x_t}(h,c)$, thus indirectly solving x_0 via Eq. (18). It is useful to take a step back to think about what x_0 represents. The value of x_0 is the intercept of the regression line on the abscissa, and since it represents a parameter for a fit to the tail of the distribution for modelling extreme ice loads of interest for design, it does not model the data corresponding to low ice loads and should not be misinterpreted as having a physical meaning. It would be beneficial to start with a parameter with clear physical meaning, so that it is possible to establish a function which reflects our physical understanding rather than establishing that purely mathematically. On the contrary, x_t is the load value at the 80% quantile, thus has clear physical meaning. Moreover, x_t appears naturally in the PDF of the tail data as shown in Eq. (14), which provides convenience for parameter estimation. Based on above argument, the approach proposed here opts for indirect modelling of x_0 through $f_{x_t}(h,c)$.

4.3. Function forms of $f_\beta(h,c)$ and $f_{x_t}(h,c)$

From Fig. 8, it can be observed that β generally increases when ice thickness grows, but the dependency on ice concentration seems to be

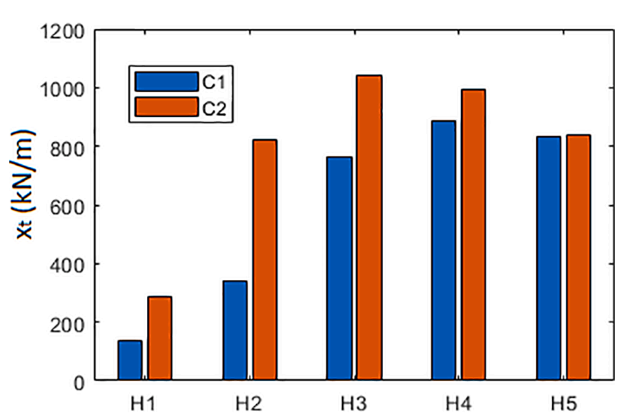

Fig. 10. Extracted x_t from the categorized dataset.

rather weak. It seems reasonable to assume β to be only dependent on thickness thus independent of ice concentration. Many publications have favored power relationship between pressure and area, e.g. [23]. A similar idea is followed here by assuming the following β-thickness relationship

$$\beta = f_\beta(h) = \theta_1 h^{\theta_2} \tag{19}$$

Here θ_1 and θ_2 are the unknown parameters to be estimated from the dataset.

The next is to determine a proper function form of x_t so that x_0 is modelled with Eq. (15). Since x_t has the same unit (kN/m) as β, both representing line loads, it is consistent to use the same form of dependence on ice thickness, i.e. $x_t = Ch^D$. From the dataset, one can easily extract x_t, i.e. the load value at the 80% quantile, which is summarized in Fig. 10.

This shows that x_t mostly increases when ice gets thicker and concentration gets higher. In other words, the line loads at the 80% percentile grows as the ice condition gets severe, which is physically reasonable. The categories with thickness over 200 cm show some difference with slightly smaller x_t values than the categories with thickness between 120 cm and 200 cm, but the decrease is much smaller comparing to x_0 in Fig. 8 and is possibly due to the variation of data as a result of small sample size. Based on above reasoning, the following function form is adopted for $f_{x_t}(h,c)$

$$x_t = f_{x_t}(h,c) = \theta_3 c h^{\theta_4 c + \theta_5} \tag{20}$$

so that the coefficient and exponent are modelled as linear functions of concentration. According to Eq. (15), x_0 is then expressed explicitly as

$$x_0 = \theta_3 c h^{\theta_4 c + \theta_5} + \theta_1 h^{\theta_2}\log 0.2 \tag{21}$$

Here θ_3, θ_4 and θ_5 are the unknown parameters to be estimated from the dataset. The condition of zero concentration leads to zero ice loads, which is physically correct. The appearance of c in the exponent takes possible coupling of h and c into account. The task is then to estimate the vector $\boldsymbol{\theta} = [\theta_1, \theta_2, \theta_3, \theta_4, \theta_5]$.

4.4. Parameter estimation based on maximum likelihood

In the categorized datasets, denote each line load by x_{ij}, where i is the index of category while j the index of the line load within category i. Denote the corresponding ice condition as (h_i, c_i). For a given set of $\boldsymbol{\theta}$, x_t and β can be calculated via Eqs. (19) and (20) for each category, denoted by $x_{t,i}$ and β_i. The number of loads in a category is denoted by n_i, and the number of loads with larger values than $x_{t,i}$ denoted by k_i. The notations are summarized in Table 3. The estimation of $\boldsymbol{\theta}$ will be carried out in two steps. In the first step, parameters related to x_t (i.e. θ_3, θ_4 and θ_5) will be estimated. Then in the second step, parameters related to β (i.e. θ_1 and θ_2) conditional on x_t will be estimated.

4.4.1. Estimation of θ_3, θ_4 and θ_5

Parameters θ_3, θ_4 and θ_5 determine the location of x_t, which divides the load distribution into two parts. There is 80% probability that a load falls below this value and 20% above. The probability that k_i out of n_i

Table 3
Notations used for parameter estimation.

Notation	Meaning
i	Index of a category
j	Index of data within each category
x_{ij}	Line load data in category i
h_i, c_i	Thickness and concentration in category i
$x_{t,i}, \beta_i$	$x_t$and β in category i
n_i	Number of loads in category i
k_i	Number of loads at the tail (i.e. $x_{ij} > x_{t,i}$) in category i

loads fall at the tail region can then be calculated with binomial distribution

$$P_i = Binomial(k_i, n_i, 0.2) = \binom{n_i}{k_i} 0.2^{k_i} 0.8^{n_i - k_i} \tag{22}$$

k_i is a function of $x_{t,i}$, thereby a function of $[\theta_3, \theta_4, \theta_5]$. The likelihood of $[\theta_3, \theta_4, \theta_5]$ to result in the whole dataset is then

$$L_{\theta_3,\theta_4,\theta_5} = \prod_{i=1}^{10} \binom{n_i}{k_i} 0.2^{k_i} 0.8^{n_i - k_i} \tag{23}$$

where 10 is the number of categories. Taking the logarithm gives

$$\log L_{\theta_3,\theta_4,\theta_5} = \sum_{i=1}^{10} \log \binom{n_i}{k_i} + k_i \log 0.2 + (n_i - k_i)\log 0.8 \tag{24}$$

The MLE solution of $[\theta_3, \theta_4, \theta_5]$ is found by numerically searching the $[\theta_3, \theta_4, \theta_5]$ which leads to maximum $\log L_{\theta_3,\theta_4,\theta_5}$. Since binomial distribution is a discrete distribution, the solutions of $[\theta_3, \theta_4, \theta_5]$ are intervals rather than single values. The $[\theta_3, \theta_4, \theta_5]$ combination which yields the maximum likelihood of $L_{\theta_1,\theta_2|\theta_3,\theta_4,\theta_5}$ in the following step is finally chosen as optimal.

4.4.2. Estimation of θ_1 and θ_2 conditional on θ_3, θ_4 and θ_5

For a given set of $[\theta_3, \theta_4, \theta_5]$, x_t can be calculated for each category. Without loss of generality and for the convenience of expression, x_{ij} is sorted in descending order so that $x_{i1}, x_{i2}, \cdots, x_{ik}$ are the data located at the tail. The likelihood of the tail data located at the measured values is then

$$\begin{aligned} L_{\theta_1,\theta_2|\theta_3,\theta_4,\theta_5} &= \prod_{i=1}^{10} \prod_{j=1}^{k_i} \frac{1}{\beta} \exp\left(-\frac{1}{\beta}(x_{ij} - x_{t,i}) \right) \\ &= \prod_{i=1}^{10} \prod_{j=1}^{k_i} \frac{1}{\beta} \exp\left(-\frac{1}{\beta}(x_{ij} - x_{t,i}) \right) \end{aligned} \tag{25}$$

Taking the logarithm and replacing β by Eq. (19) yield

$$\log\left(L_{\theta_1,\theta_2|\theta_3,\theta_4,\theta_5}\right) = -N\log\theta_1 - \theta_2 \sum_{i=1}^{10} k_i \log h_i - \theta_1^{-1} \sum_{i=1}^{10} \sum_{j=1}^{k_i} h_i^{-\theta_2}(x_{ij} - x_{t,i}) \tag{26}$$

The optimal θ_1 and θ_2 resulting in the maximum likelihood can be found by taking the derivation of $\log\left(L_{\theta_1,\theta_2|\theta_3,\theta_4,\theta_5}\right)$ with regards to θ_1 and θ_2 and equals them to zero, which gives

$$\theta_1 = \frac{\sum_{i=1}^{10} \sum_{j=1}^{k_i} h_i^{-\theta_2}(x_{ij} - x_{t,i})}{N} \tag{27}$$

$$-\sum_{i=1}^{10} k_i \log h_i - \theta_1^{-1} \sum_{i=1}^{10} \sum_{j=1}^{k_i} h_i^{-\theta_2}(x_{ij} - x_{t,i}) \log h_i = 0 \tag{28}$$

Solving these non-linear equations gives the solution to the optimal θ_1 and θ_2 conditional on optimized $[\theta_3, \theta_4, \theta_5]$. The MLE solution of $\boldsymbol{\theta}$ is now obtained through these two steps.

4.5. Parameter estimation based on probability paper

Estimation based on maximum likelihood utilized the inherent probabilistic nature of the data. A less rigorous, but easier to understand and solve, approach is to estimate parameters based on probability paper, which was adopted by Jordaan et al. [9]. Unlike maximum likelihood estimation where whether a data point locates at the tail is probabilistic, with probability paper the upper 20% of data within each category are assumed to be in the tail with certainty. In addition to the notations defined in Table 3, we further define y as the negative logarithm of the probability of exceedance (i.e. $-\log P_e$), see Fig. 1, so that the estimated line load $\hat{x}$ can be expressed as:

$$\hat{x} = \beta y + x_0 = f_\beta(h, c)y + f_{x_0}(h, c) \tag{29}$$

With Eqs. (19) and (20), this can be re-written as

$$\hat{x} = \theta_1 h^{\theta_2} y' + \theta_3 c h^{\theta_4 c + \theta_5} \tag{30}$$

where y' has been used to replace $y + \log 0.2$.

After identifying the data at the tail region of each category, the tail data of all the categories are merged into a whole dataset. The dataset includes a set of (Y, X, h, c) vectors where Y equals $-\log p_e$ which relates to the return period and X is a measured line load value. If each data point is labelled as (y_s, x_s, h_s, c_s), the sum-of-square error of the regression can be expressed as

$$E = \sum_{s=1}^{N} \frac{1}{2}(x_s - \hat{x}_s)^2 \tag{31}$$

where N is the size of the merged tail dataset; $\hat{x}_s$ relates to y_s, h_s, c_s via Eq. (30). To minimize E, the derivates of E with respect to θ in the first model or $\mathbf{w}$ in the second model should equal zero. In the first model with expert knowledge, this yields

$$\frac{dE}{d\theta_k} = \sum_{s=1}^{N} (x_s - \hat{x}_s) y' \frac{d\beta_s}{d\theta_t} = 0, \quad where\ t = 1, 2 \tag{32}$$

$$\frac{dE}{d\theta_k} = \sum_{s=1}^{N} (x_s - \hat{x}_s) y' \frac{dx_{t,s}}{d\theta_t} = 0, \quad where\ t = 3, 4, 5 \tag{33}$$

This consists of a system of five non-linear equations with five unknown variables. The parameters θ_1 to θ_5 can then be obtained by solving this system of non-linear equations.

4.6. Uncertainty quantification

Both the above approaches based on maximum likelihood and probability paper give point estimation of the parameters. To assess the uncertainty associated with the estimated θ parameters, Bayesian approach is adopted. According to Bayes's theorem,

$$f(\mathbf{X}|\theta)p(\theta) = f(\theta|\mathbf{X})f(\mathbf{X}) \tag{34}$$

where $f(\mathbf{X}|\theta)$ is the likelihood, $f(\theta)$ the prior distribution and $f(\theta|\mathbf{X})$ is the posterior distribution. With no prior knowledge on θ, $f(\theta)$ is set as constant, which yields

$$f(\theta|\mathbf{X}) \propto f(\mathbf{X}|\theta) \tag{35}$$

By normalization, this results in

$$f(\theta|\mathbf{X}) = \frac{f(\mathbf{X}|\theta)}{\int f(\mathbf{X}|\theta)d\theta} \tag{36}$$

Specifically, following Eq. (23) and Eq. (25),

$$f(\theta_3, \theta_4, \theta_5|\mathbf{X}) = \frac{f(\mathbf{X}|\theta_3, \theta_4, \theta_5)}{\int f(\mathbf{X}|\theta_3, \theta_4, \theta_5)d[\theta_3, \theta_4, \theta_5]} = \frac{L_{\theta_3,\theta_4,\theta_5}}{\int L_{\theta_3,\theta_4,\theta_5} d[\theta_3, \theta_4, \theta_5]} \tag{37}$$

$$\begin{aligned} f(\theta_1, \theta_2|\mathbf{X}, \theta_3, \theta_4, \theta_5) &= \frac{f(\mathbf{X}|\theta_1, \theta_2, \theta_3, \theta_4, \theta_5)}{\int f(\mathbf{X}|\theta_1, \theta_2, \theta_3, \theta_4, \theta_5)d[\theta_1, \theta_2]} \\ &= \frac{L_{\theta_1,\theta_2|\theta_3,\theta_4,\theta_5}}{\int L_{\theta_1,\theta_2|\theta_3,\theta_4,\theta_5} d[\theta_1, \theta_2]} \end{aligned} \tag{38}$$

It is difficult to derive closed-form solutions for Eqs. (37) and (38), but $f(\theta_3, \theta_4, \theta_5|\mathbf{X})$ and $f(\theta_1, \theta_2|\mathbf{X}, \theta_3, \theta_4, \theta_5)$ can be computed numerically with discretized θ values. The uncertainty in the estimated θ is then quantified.

To assess the influence of uncertainty in parameter estimation on the estimation of long-term ice loads, we will evaluate the predictive distribution given as per

$$f(x_{extreme}|\mathbf{X}) = f(\theta_3, \theta_4, \theta_5|\mathbf{X}) f(\theta_1, \theta_2|\mathbf{X}, \theta_3, \theta_4, \theta_5) f(x_{extreme}|\mathbf{X}, \theta_3, \theta_4, \theta_5, \theta_1, \theta_2) \tag{39}$$

using Monte Carlo simulation following the below procedure:

1. Randomly generate $\theta_3, \theta_4, \theta_5$ according to $f(\theta_3, \theta_4, \theta_5|\mathbf{X})$.
2. Randomly generate θ_1, θ_2 according to $f(\theta_1, \theta_2|\mathbf{X}, \theta_3, \theta_4, \theta_5)$.
3. Calculate β_i and $x_{t,i}$ based on generated θ and given h and c, thereby giving $x_{0,i}$.
4. Randomly generate a long-term extreme value $x_{extreme}$ based on the distribution given in Eq. (10), with calculated β_i and $x_{0,i}$.
5. Repeat the above step for 10^4 times and get the predictive distribution of long-term extremes which considers the uncertainty in parameter estimation.

5. Results and validation

5.1. Results of parameter estimation

The parameter estimation procedures based on maximum likelihood and probability paper as described in Section 4 are applied to the ice loads measured on the two bow frames, namely frame #134 and frame #134.5. Three cases are investigated: (i) frame #134.5; (ii) frame #134; and (iii) combined frame #134 and #134.5. The first two correspond to single frames with frame spacing 0.4 m and the last concerns two frames with a span of 0.8 m. Fig. 11 presents the results of regressions by both methods described in Section 4.2, plotted with the dataset. The regression lines from both estimation methods generally reflect the magnitudes and trends of the dataset, with most of the data spread close to the lines. Some regression lines, e.g. C2H1, give systematically larger load values than the data. This is because of the deviation in the estimated x_t values, which shift the regression lines along positive or negative x-direction. Since each data point is assigned with equal weight during the estimation, the regression lines are obviously better fitted to the categories with more data, e.g. C2H2, compared to categories with few data, e.g. C2H1. The overall good fitting indicates the proposed β and x_0 modelling methodology with both estimation methods can well capture the feature of the training dataset.

Table 4 summarizes the obtained functions of β and x_0 by both estimation methods for the three cases. The parameters estimated with different methods differ, but the difference is relatively small. With both methods, the estimated parameters for frame #134 and #134.5 are similar, which is expected since frame #134 and #134.5 are adjacent frames. The β functions are plotted in Fig. 12 for visualization using Frame #134.5 as an example. For an easy comparison to the α-thickness curves in the literature, the β curves are converted to α (i.e. pressure) with an assumption that the contact height equals 0.3 times ice thickness following Shamaei et al. [8]. The individual fitting results from Fig. 8 are also shown as scatter for comparison. Similarly, the x_0 functions by both models are plotted in Fig. 13. The obtained functions correctly reflect our physical understanding that β increases when ice condition gets heavier and α decreases as a function of thickness.

5.2. Validation with six-year data

5.2.1. Qualitative comparison with six-year data

Two different approaches are adopted here to validate the obtained models with six years of data. In the first approach, the six-year data are categorized in the same way as was done to the 2018/19 data. The line load data falling into each category are then ranked and plotted versus the corresponding negative $\log p_e$. After that the β and x_0 values are calculated by the resulting functions in Table 4 obtained from the 2018/19 data. The line of each category characterized by β and x_0 is then plotted and compared with the ranked measurement. The results are shown in Fig. 14. The aim of this comparison is to conduct a qualitative visual examination of how well the models obtained from the 2018/19 voyage can describe the data obtained from the six-year voyages. The plots visually demonstrate that the linear regression lines obtained from fitting to one-year measurement can be well generalized to multiple year measurements. This gives evidence to the proposed Method as the tool

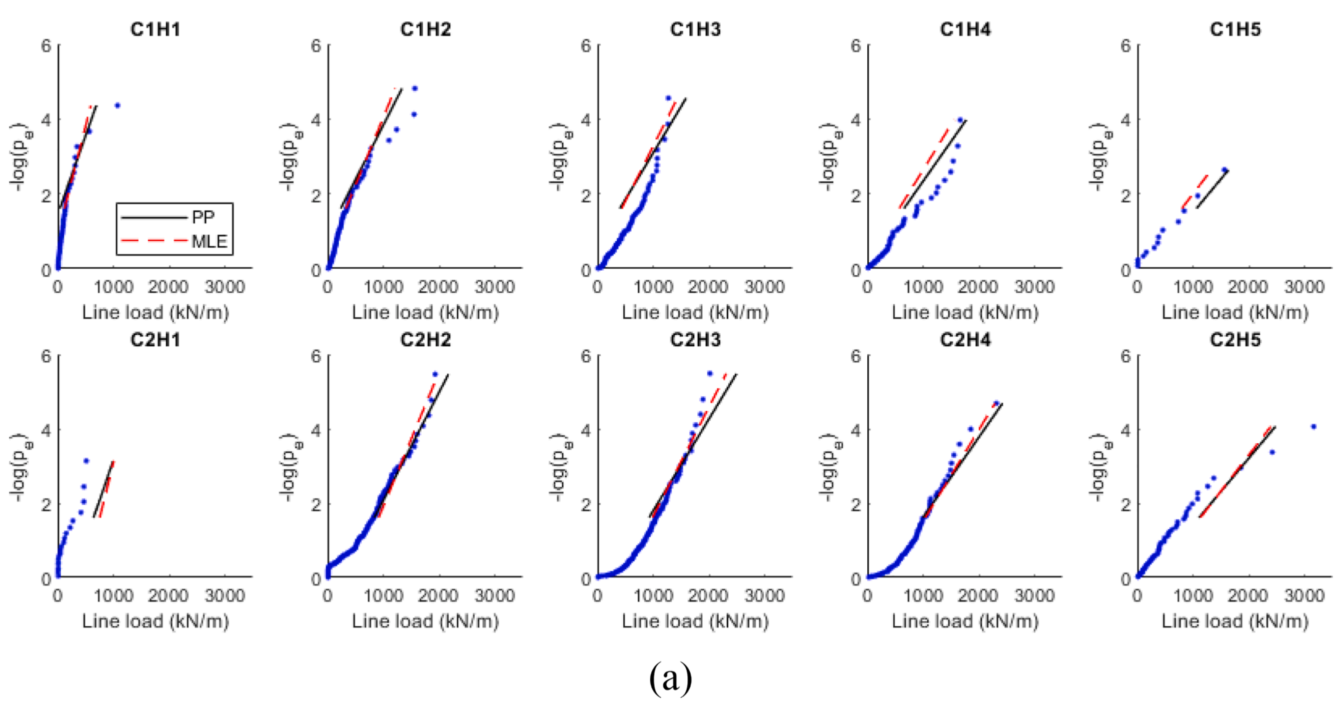

Fig. 11. Regression to the dataset, (a) frame #134.5; (b) frame #134; (c) combination of frame #134.5 and #134.

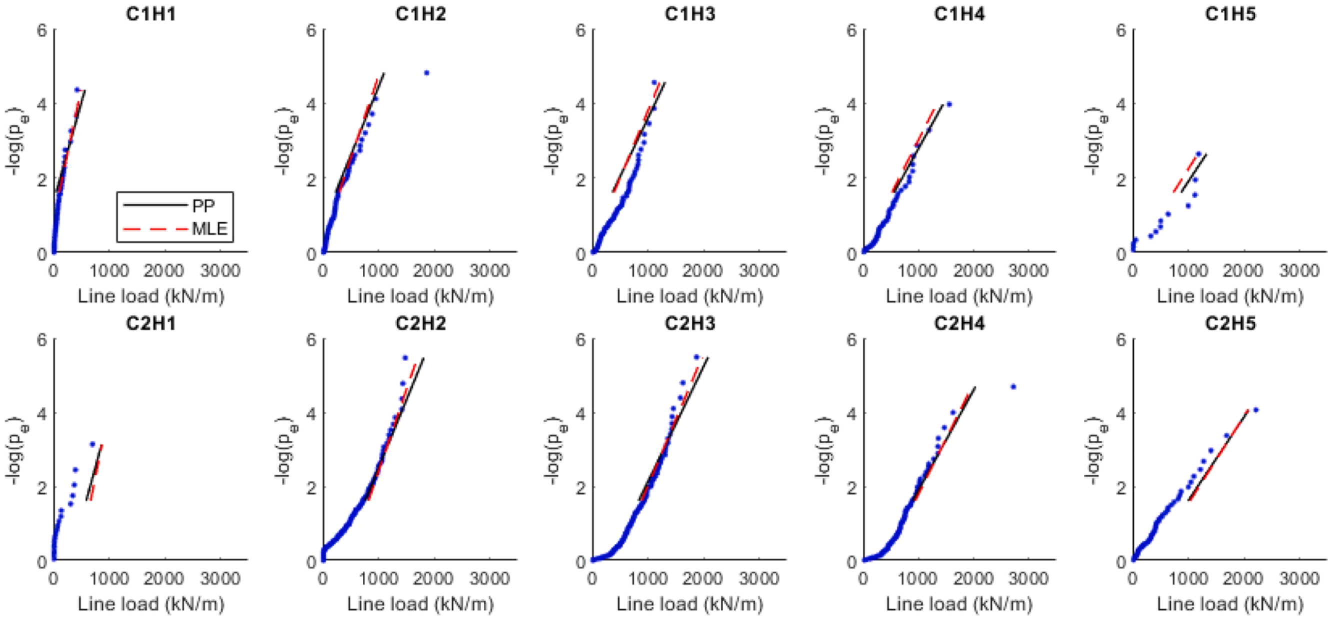

(b)

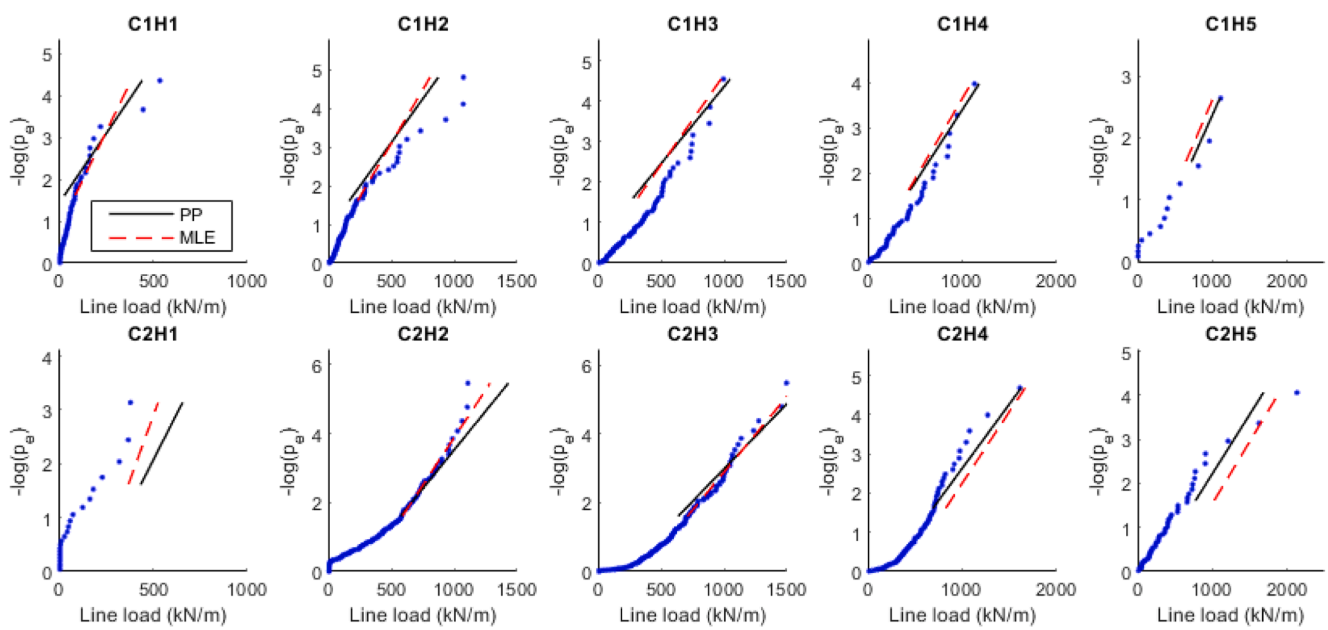

(c)

Fig. 11. (*continued*).

Table 4
Summary of the obtained β, x_t and x_0 functions.

	Frame number	β	x_t	x_0
MLE	#134.5	$343h^{0.442}$	$10.5ch^{-0.0047c+0.59}$	$x_{0.8}+\beta\log 0.2$
	#134	$282h^{0.443}$	$9.48ch^{-0.0049c+0.62}$	
	#134.5 & #134	$228h^{0.48}$	$7.60ch^{-0.0014c+0.52}$	
Prob.paper	#134.5	$407h^{0.344}$	$9.86ch^{-0.0136c+1.47}$	
	#134	$323h^{0.346}$	$8.91ch^{-0.0109c+1.21}$	
	#134.5 & #134	$267h^{0.354}$	$6.77ch^{-0.0127c+1.43}$	

for the estimation of long-term extreme loads. The lines agree better with the measurement in the categories where more 2018/19 data have been used to train the model, e.g. C2H2, but not so well with those where fewer data have been used to train the model, e.g. C2H1. It should be noted that the line load values given by the regression lines are the characteristic extremes (i.e. z_m in Fig. 2), which is the most likely value corresponding to certain return period (i.e. $\frac{1}{p_e}$), instead of a definite value. The results inherently contain probabilistic meaning according to Eq. (6).

It can be noticed that in category C2H1 and C2H2, the maxima obtained from the measurement (marked in circles in Fig. 14) are significantly higher than the estimated characteristic extremes. These values are also significantly larger than the second largest values in the

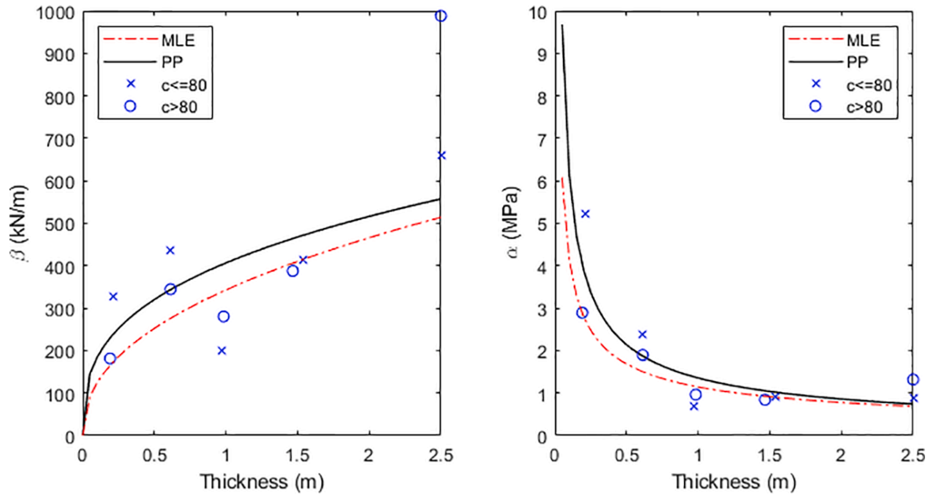

Fig. 12. Examples of obtained β functions (left) and converted α functions (right) assuming $0.3h$ as contact height, estimated with probability paper (PP) and maximum likelihood estimation (MLE), the scatters showing the values obtained from Fig. 8.

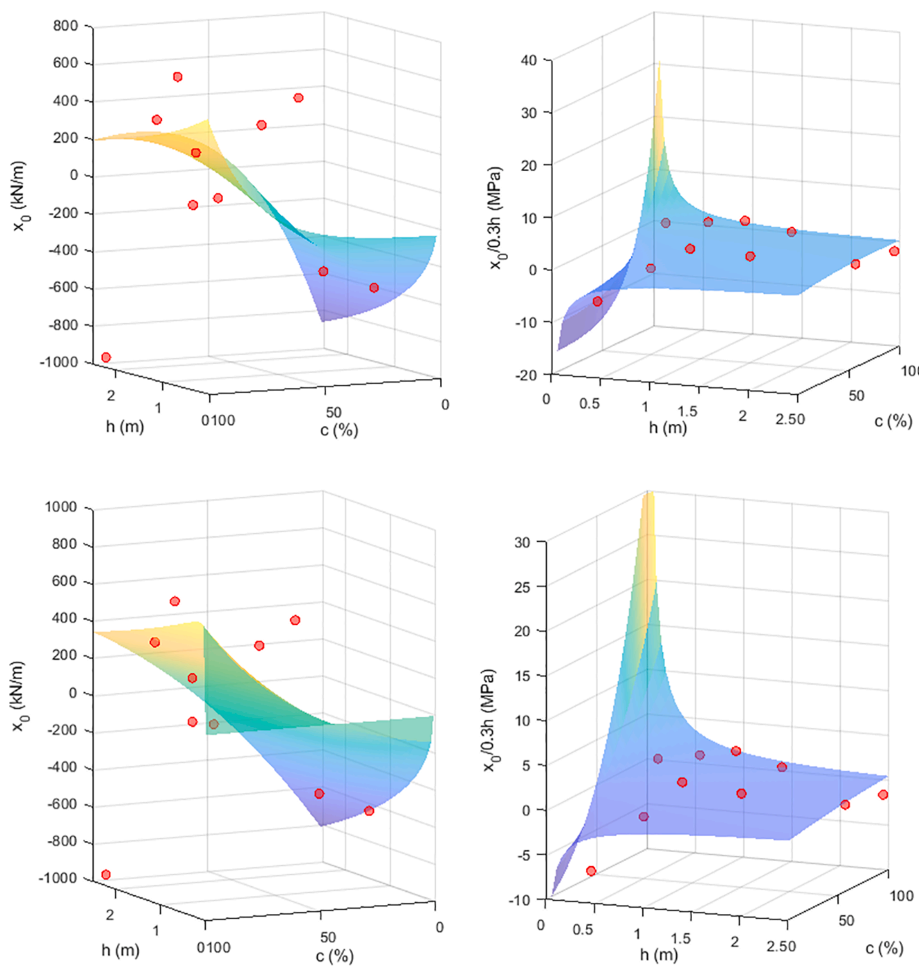

Fig. 13. Examples of obtained x_0 functions (left) and converted pressure values (right) assuming $0.3h$ as contact height, showing estimation with probability paper (upper) and maximum likelihood (bottom), the scatters showing the values obtained from Fig. 8.

corresponding categories. There can be at least two possible reasons for this. The first is that some low-probability events happened, which yield rather large loads. The second is that these are outliers arising from misclassification. Since thickness and concentration are observed values in our dataset, there are inevitably certain misclassified data after categorization. It is then possible that these largely deviated values should actually fall into categories with higher thickness, but the actual maximum thickness is not successfully observed during these events. It is worth mentioning that the method is in fact not sensitive to such few misclassifications. This is because as will be demonstrated in Section

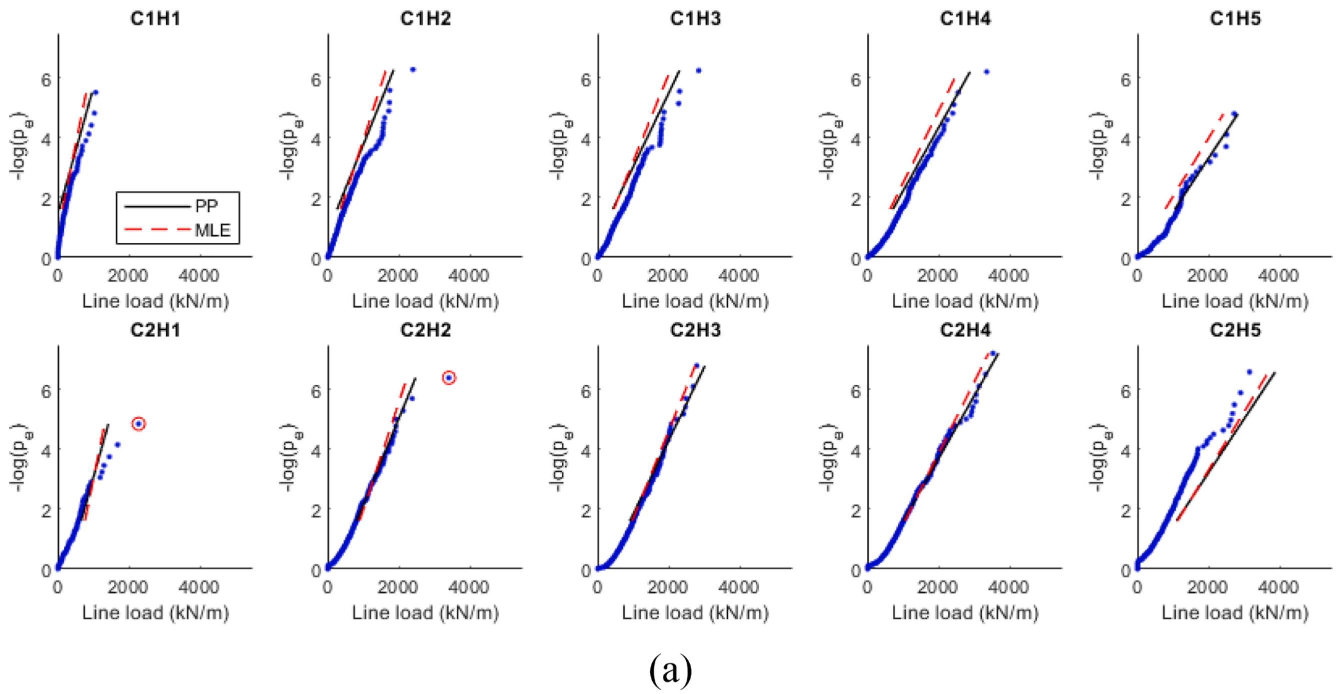

Fig. 14. Qualitative validation of the obtained β and x_0 functions against six-year measurement, (a) frame #134.5; (b) frame #134; (c) combination of frame #134.5 and #134.

5.2.2, all the categories are considered simultaneously when making estimations. A small number of misclassifications only result in minor changes in the number of events in the categories, which leads to little effect on the estimations.

5.2.2. Quantitative comparison between estimations and measurements

The second validation approach is quantitative. The resulting models are applied to make estimations on the maximum ice loads encountered during each of the six-year voyages, as well as all the entire six-year voyages. The estimations include the characteristic extreme values as well as the 95% quantiles. The estimations are then compared with the measurements to check for agreement. We will take frame #134.5 of the 2014/15 voyage data as an example, with the resulting functions estimated by probability paper to demonstrate. In this voyage, there are in total 1087 ten-minute events, which are spread in the categories as shown in Table 5. One can as well adopt a different categorization strategy; the principle remains the same. The next step is to calculate the mean ice thickness and concentration within each category. Here these are calculated from the visual observation information. One can also take the medians of the thickness and concentration intervals in case of no exact measurement. Based on thickness and concentration, β and x_0 can be calculated according to the results in Table 4. Now $F_Q(q)$ in Eq. (10) can be evaluated in terms of any given q value. The characteristic extreme load q_m can be found numerically according to Eq. (11). In addition to this most likely extreme value, we also estimate the quantiles in order to account for the randomness. Here we evaluate the 95% interval by finding the 2.5% and 97.5% quantiles, denoted by $q_{2.5}$ and $q_{97.5}$. These are calculated numerically by setting $F_Q(q)$ to 2.5% and 97.5%. The estimated characteristic maximum line load encountered in the 2014/15 voyage is 3143kN/m, with 95% probability to be located within [2526, 4993]kN/m. The measured maximum load during this voyage is 3536kN/m, which falls into the interval and is close to the characteristic maximum value. The estimation with functions obtained through maximum likelihood gives 2906kN/m as the characteristic maximum and [2357, 4598]kN/m as the 95% confidence interval, which is similar to the results obtained via probability paper.

The same procedure is applied to other frame cases and other voyages, with resulting functions by both probability paper and maximum likelihood. The results are summarized in Fig. 15, where the error bar shows the 95% intervals and scatters show the characteristic extreme values and the measured maxima. In most cases, the measurement locates within the 95% interval, mostly not far from the characteristic extremes. There are only two cases with probability paper estimation and one cases with maximum likelihood estimation where the load is outside the 95% interval. This indicates that the models obtained from the 2018/19 voyage give generally reasonable estimations of the maxima encountered in other voyages. Overall, the estimations of maxima by both estimation methods are rather similar.

5.3. Uncertainty assessment

Here we use the results obtained from frame #134.5 as the example to examine the influence of uncertainty in model parameters on the estimation performance. Following Section 4.6, the joint probability of $\theta_3,\theta_4,\theta_5$, i.e. $f(\theta_3,\theta_4,\theta_5|\mathbf{X})$, and conditional probability $f(\theta_1,\theta_2|\mathbf{X},\theta_3,\theta_4,\theta_5)$ can be numerically evaluated. Fig. 16 plots the marginal probability of $\theta_3,\theta_4,\theta_5$ and that of θ_1,θ_2 at optimal $\theta_3,\theta_4,\theta_5$, to illustrate the uncertainty in model parameters.

Uncertainties in model parameters leads to uncertainties in β and x_0 given certain combination of thickness and concentration. Using the six-year loads on frame #134.5 as an example. The resulting joint probabilities of β and x_0 of categories C1H1 and C2H1 are shown as examples by histograms in Fig. 17. This is obtained by randomly generating $\theta_3,\theta_4,\theta_5$ according to $f(\theta_3,\theta_4,\theta_5|\mathbf{X})$ and θ_1,θ_2 according to $f(\theta_1,\theta_2|\mathbf{X},\theta_3,\theta_4,\theta_5)$, then calculating β and x_0 with the θ parameters. As shown in the figure, β and x_0 are naturally correlated.

Uncertainties in β and x_0 eventually leads to uncertainties in the estimation of extreme ice loads. This will be demonstrated via two aspects. First, uncertainty in the characteristic extreme loads of the six-year voyages is investigated because this is a value which may be used in design. The characteristic extreme load is a definite function of β and x_0 as given in Eq. (7), therefore its uncertainty depends on the joint

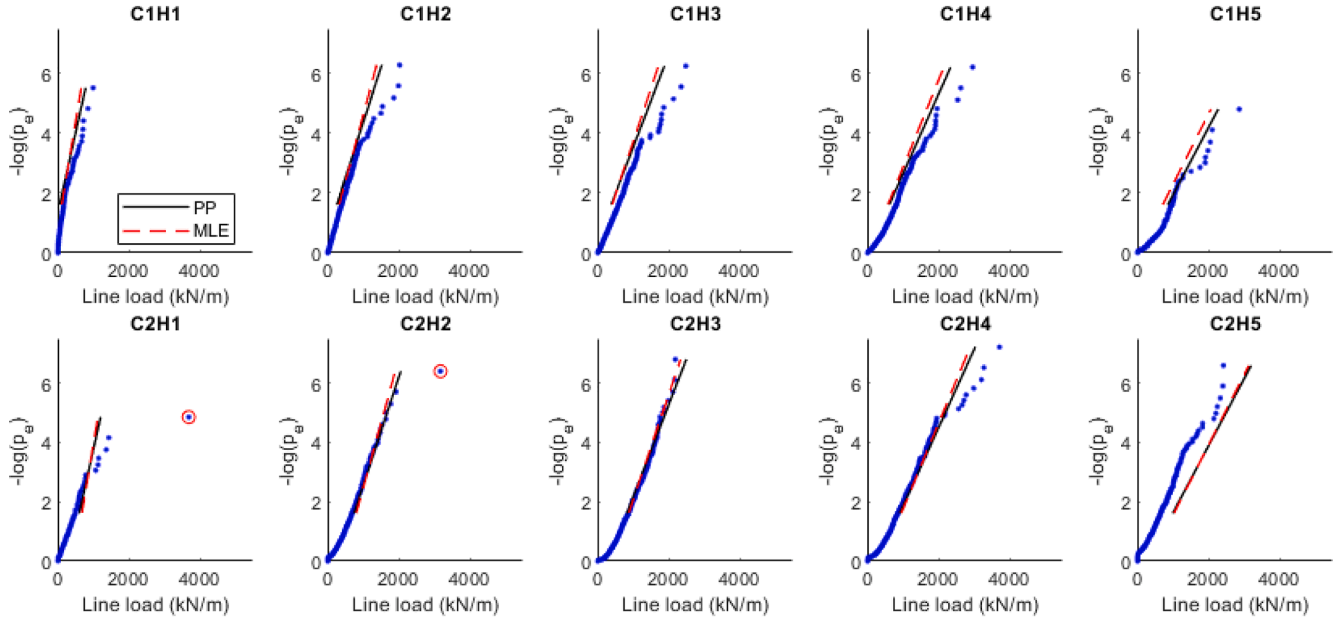

(b)

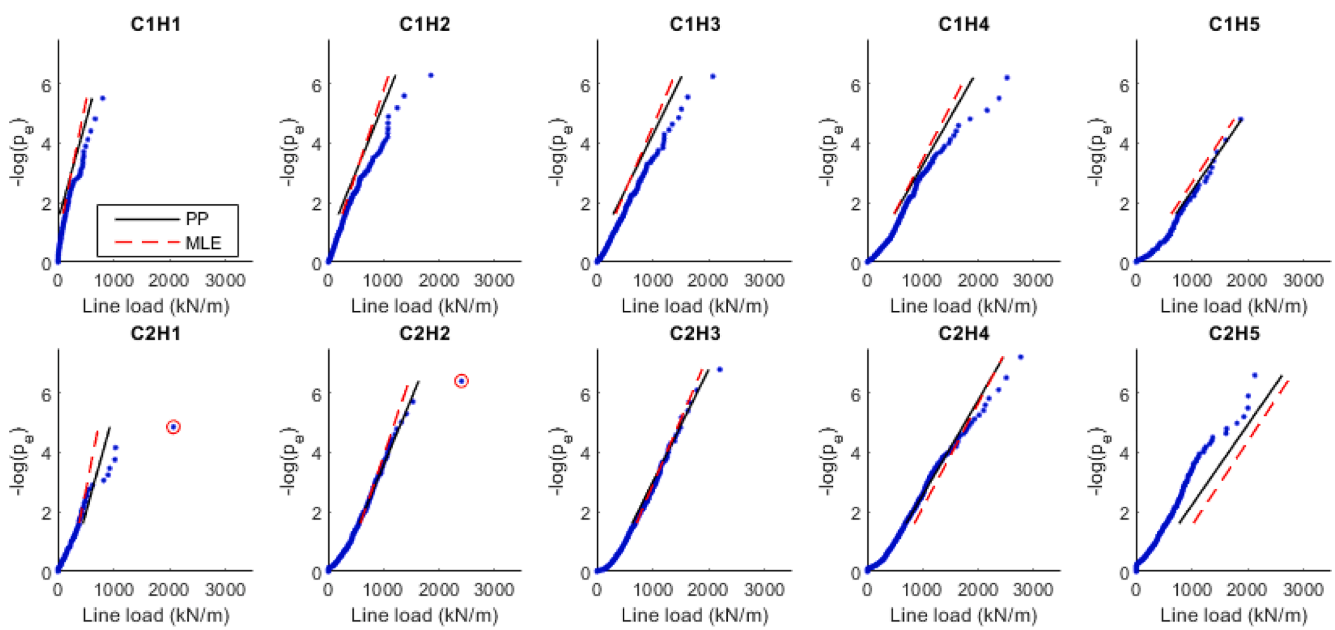

(c)

Fig. 14. (*continued*).

Table 5
Example of maximum load estimation with 2014/15 voyage data.

Category	No. of events	h(m)	c(%)	β(kN/m)	x_0 (kN/m)	q_m (kN/m)	$[q_{2.5}, q_{97.5}]$ (kN/m)	Measured max. (kN/m)
C1H1	73	0.17	20	237	−339	3143	[2526,4993]	3536
C2H1	19	0.15	91	230	274			
C1H2	99	0.59	49	342	−312			
C2H2	97	0.65	90	343	287			
C1H3	73	0.97	43	403	−245			
C2H3	177	0.98	93	404	275			
C1H4	19	1.49	53	471	−101			
C2H4	175	1.55	94	464	247			
C1H5	25	2.5	54	558	164			
C2H5	60	2.5	94	558	209			

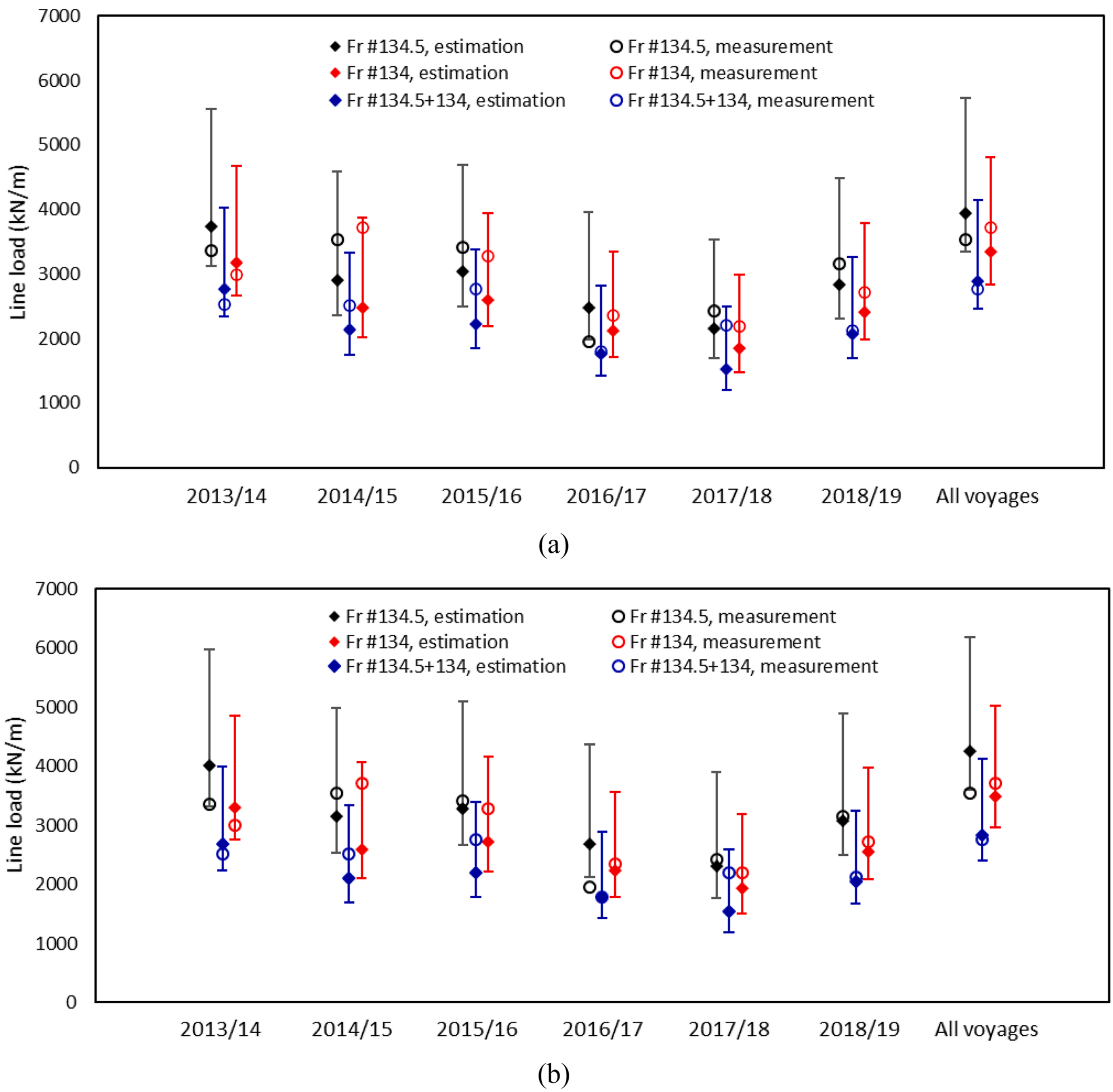

Fig. 15. Estimated and measured maximum loads on frame #134.5, #134 and their combination, of the individual voyages as well as all voyages, estimated with (a) probability paper and (b) maximum likelihood.

probability distribution of β and x_0. This is shown in Fig. 18 by randomly generating 10^4 β and x_0 and calculating the characteristic extreme accordingly. The standard deviation of the randomly generated characteristic extremes is 311kN/m, which is about 8% of the characteristic extreme load value calculated with MLE solutions.

Second, the predictive distribution given in Eq. (39) is evaluated using Monte Carlo simulation following the procedure described in Section 4.6. The predictive distribution of the maximum load during the six-year voyages, which takes model parameter uncertainty into account, is plotted in Fig. 19, together with the estimated extreme distribution using maximum likelihood solution. Despite of the uncertainty in model parameters, the predictive distribution is rather similar to the distribution obtained with maximum likelihood solution. The $[q_{2.5}, q_{97.5}]$ interval after accounting for uncertainty is [3270, 5935]kN/m, which is only slightly wider than that obtained with MLE solution ([3342, 5731] kN/m). This is to some extent understandable because the standard deviation of the extreme distribution with exponential distribution as parent distribution is positively correlated with β, therefore the variation in β does not necessarily widen the $[q_{2.5}, q_{97.5}]$ interval. The uncertainty in model parameters then leads to little difference between the predictive extreme distribution and the extreme distribution using point estimation results. This implies that for practical use, we could simply apply the point estimation solutions either via probability paper or maximum likelihood without accounting for uncertainty in model parameters.

5.4. Model trained with data from a different year

In order to understand how the obtained model and its extreme load estimation are affected by the yearly variation of the training dataset,

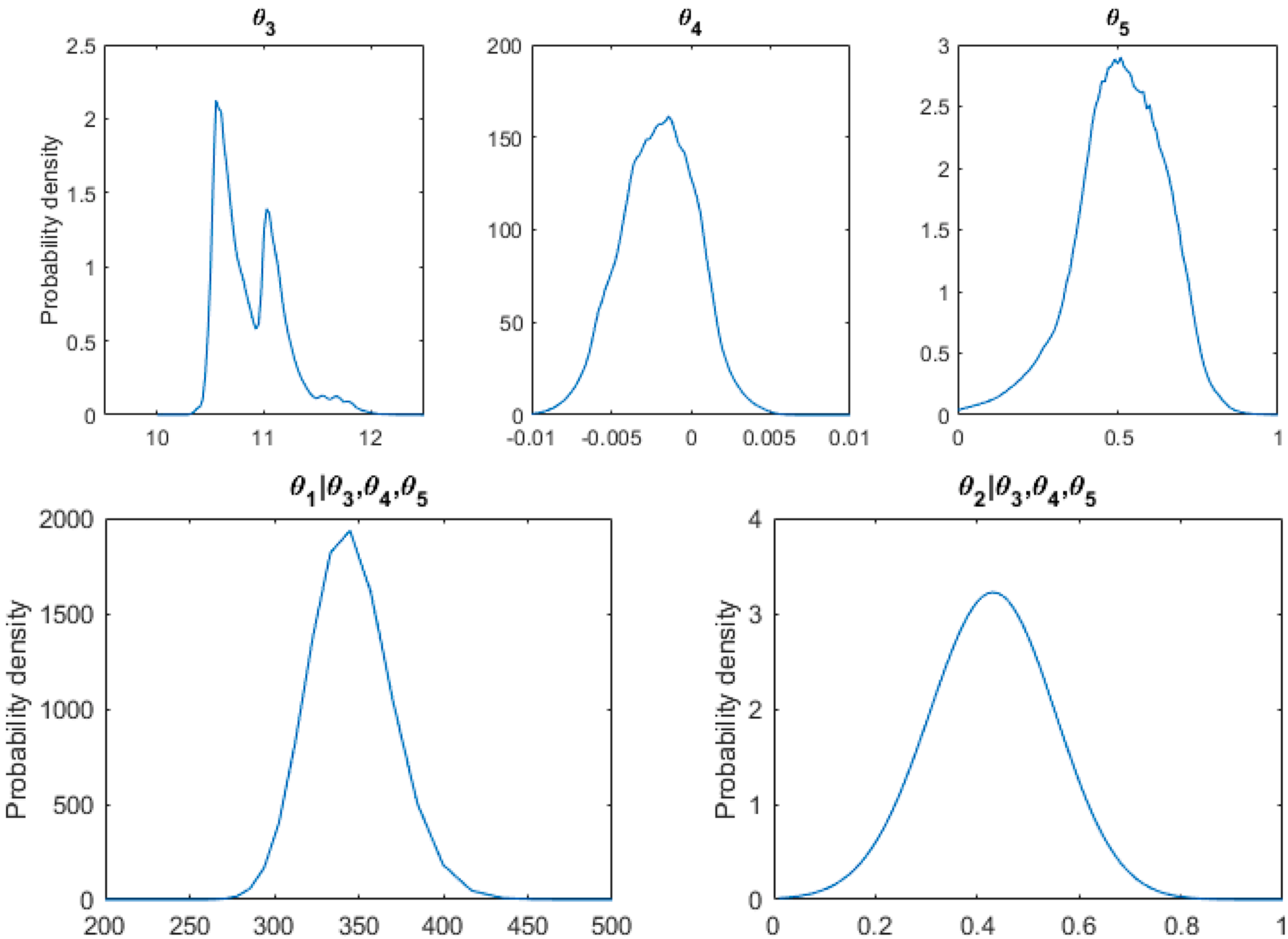

Fig. 16. Uncertainty in the estimated model parameters, presented via marginal probability distributions.

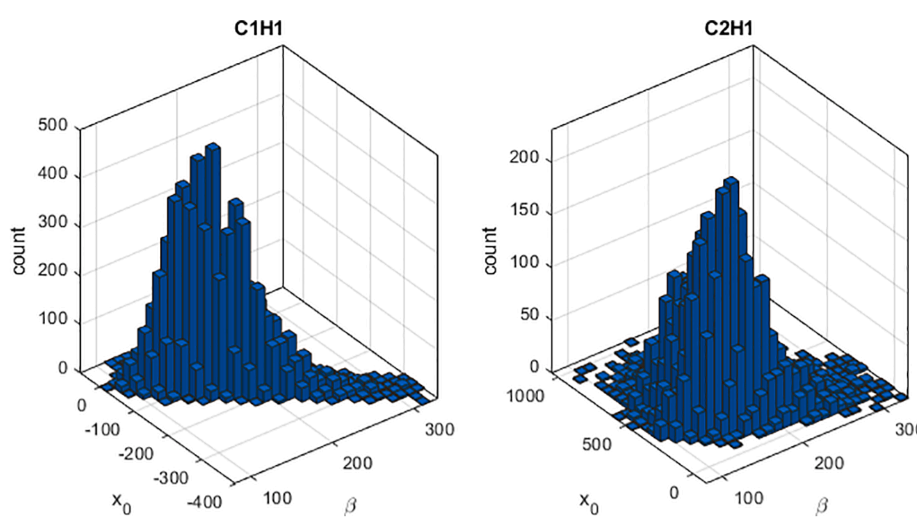

Fig. 17. Examples of uncertainty in β and.x_0

the same procedure as previously presented is adopted on the 2014/15 dataset. Frame #134.5 is used as an example, with parameters estimated by MLE. Table 6 summarized the obtained functions, with those obtained from the 2018/19 dataset listed as well for comparison. The resulting functions differs apparently on the estimated parameters, but the difference is not dramatic. The models are then applied for the estimation of yearly and six-year maxima following the same procedure as previously presented. The results are shown in Fig. 20. The estimations using the 2014/15 dataset as training dataset gives approximately 20% larger load values than those estimated based on the 2018/19 dataset. The estimation performance is not as good as the model on 2018/19 dataset, but still most of the yearly maxima are estimated

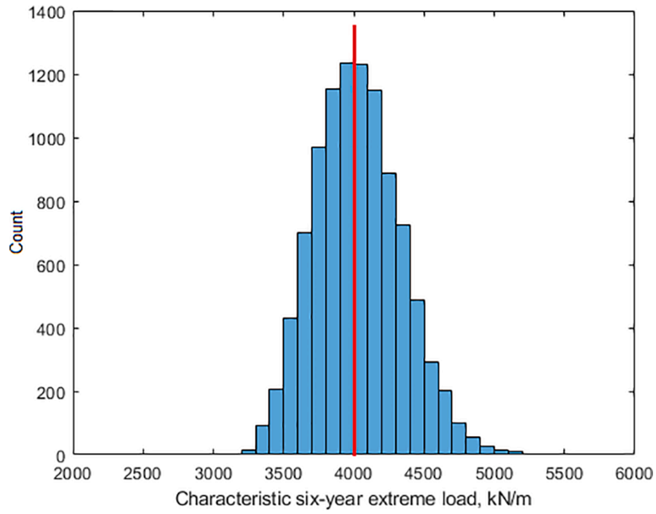

Fig. 18. Histogram of random samples showing the uncertainty in characteristic extreme load; red solid line showing the location of characteristic extreme load using maximum likelihood estimation. (For interpretation of the references to colour in this figure legend, the reader is referred to the web version of this article.)

reasonably.

Fig. 20 also shows that the 2014/15 yearly maximum load deviates most from the estimations based on 2018/19 model, implying that the 2014/15 dataset may have the largest difference comparing to the 2018/19 dataset. This indicates that the variation in estimations showing in Fig. 20 may approximately represent an upper limit among other datasets.

6. Demonstration of the extended EMM as a design tool

The ultimate aim of the proposed model is to assist ship design for the estimation of design load. Here a demonstration of the procedure to define the life-time extreme load is given. This is similar to the procedure in Section 5.2.2 but with different context. Suppose the design of an imaginary ship which will operate in the similar area as S.A. Agulhas II, where navigation in ice is needed. Annually, the ship operates in different ice conditions with different distance, which is summarized in Table 7. The life of the ship will be 25 years so the life-time exposure can be calculated based on the operation distance and speed profile, listed in Table 7.

The aim is to estimate the lifetime maximum line load at the bow area where the frame angle is similar to the #134.5 frame of S.A. Agulhas II. Similarly to Section 5.2.2, theβ and x_0 of each category can be calculated with the results in Table 4, here the resulting functions obtained through probability paper is used as an example. The results are listed in Table 8. The CDF of the life-time extreme line load, q, can then be calculated by Eq. (10). The PDF of q can be obtained by taking the derivative of the CDF, plotted in Fig. 21. One can find the characteristic extreme value q_m by finding the mode of the PDF, which is 4104kN/m in this case. One can also find the extreme load corresponding to a certain level of probability of exceedance, e.g. 10^{-2}, which gives 6184kN/m as q_e. This means that there is 1% possibility that the ship will encounter loads higher than 6184kN/m during its lifetime.

The obtained results can then serve reliability-based structural design, for which the safety factor can be calculated based on the probability of extreme loads and structural resilience. The results also serve the concept of goal-based design [24], which determines a ship's design load based on its operational area and exposure to ice conditions with different severity.

7. Discussion

7.1. Validity of the extended EMM

The results presented in Section 5 indicates that the proposed method is valid. This has been revealed by examining in-sample performance and by comparing to out-of-sample long-term measurements.

Table 6
Summary of the obtained β, x_t and x_0 functions.

	β	x_t
2014/15	$423h^{0.291}$	$12.8ch^{-0.0018c+0.32}$
2018/19	$343h^{0.442}$	$10.5ch^{-0.0047c+0.59}$

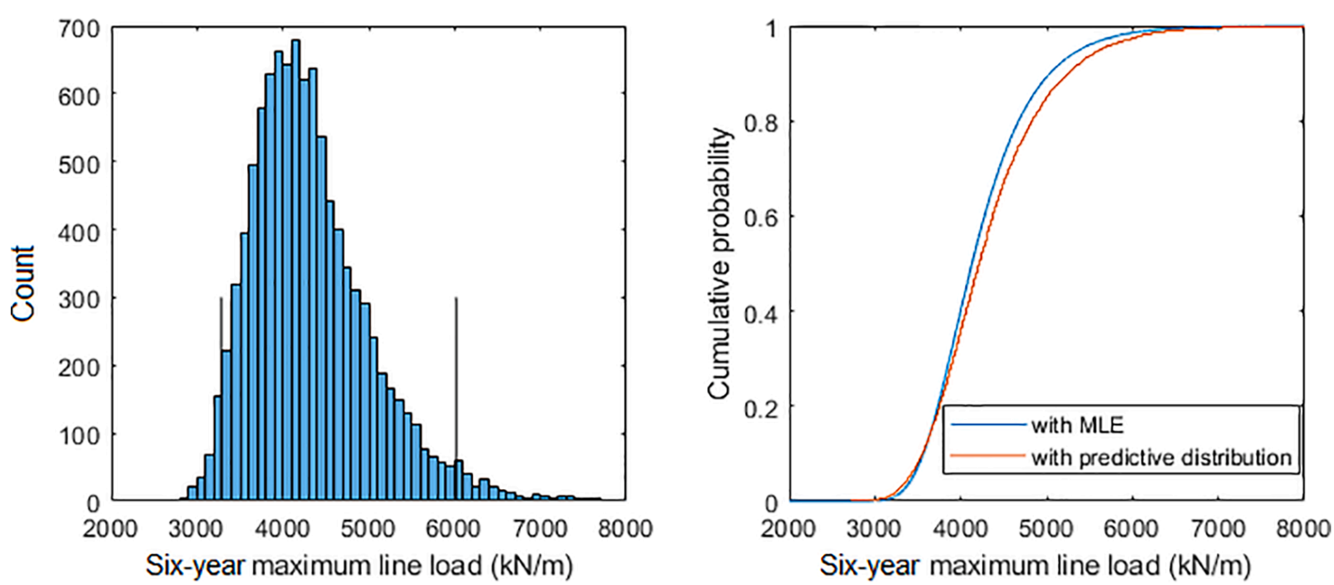

Fig. 19. Left: histogram of the six-year maxima samples randomly generated according to the predictive distribution given by Eq. (39), solid lines showing the location at 2.5% and 97.5% percentile; Right: the cumulative distribution function of the six-year maxima obtained with MLE, and the empirical cumulative distribution function of the random samples shown in the left figure.

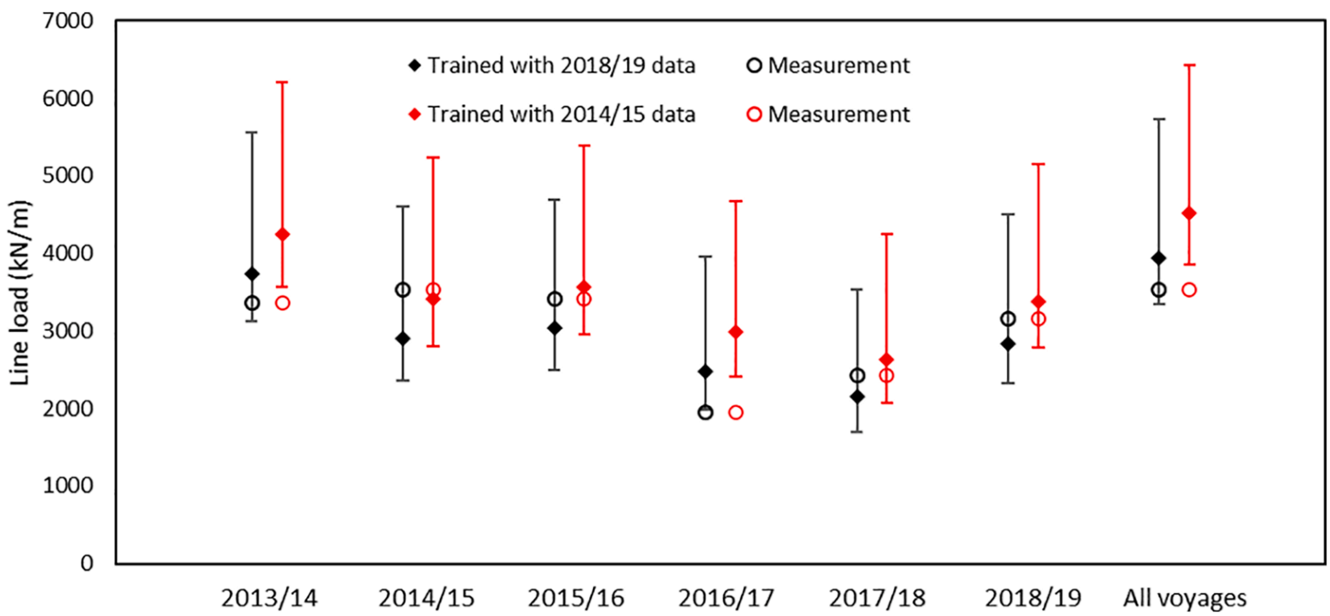

Fig. 20. Comparison of estimations of yearly and six-year maxima using model obtained based on different training dataset.

Table 7
Exposure calculation of the imaginary ship travelling in different ice condition categories.

	Annual operation distance	Speed profile	Operation time	Annual Exposure	Lifetime exposure (N_i)
C1H1	50 km	5 m/s	167 min	16.7	418
C2H1	100 km	4 m/s	417 min	41.7	1043
C1H2	150 km	4 m/s	625 min	62.5	1563
C2H2	200 km	2 m/s	1667 min	166.7	4168
C1H3	150 km	3 m/s	833 min	83.3	2083
C2H3	150 km	1.5 m/s	1667 min	166.7	4168
C1H4	100 km	2 m/s	833 min	83.3	2083
C2H4	50 km	1 m/s	833 min	83.3	2083
C1H5	0 km	–	0	0	0
C2H6	0 km	–	0	0	0

Table 8
Estimation of the life-time extreme line load.

	h(m)	c(%)	β(kN/m)	x_0 (kN/m)	N_i (Life-time exposure)	q_m (kN/m)	$q_e$with $p_e = 10^{-2}$ (kN/m)
C1H1	0.2	40	164	106	418	4104	6184
C2H1	0.2	90	164	376	1043		
C1H2	0.6	40	285	63	1563		
C2H2	0.6	90	285	361	4168		
C1H3	1.0	40	367	20	2083		
C2H3	1.0	90	367	327	4168		
C1H4	1.6	40	465	−40	2083		
C2H4	1.6	90	465	273	2083		
C1H5	2.5	40	581	−121	0		
C2H5	2.5	90	581	194	0		

Both shows that the line load distribution at the tails can be reasonably captured by the trained models. The validation also indicates that the model obtained from 2018/19 voyage gives reasonable estimation on the maximum line loads encountered during other years. Compared to the original EMM which was proposed for pressure measurement by loading panels, the extended EMM is more suitable for the line load measurement converted from strain gauges combining with visually observed ice condition. The thickness and concentration of ice can be

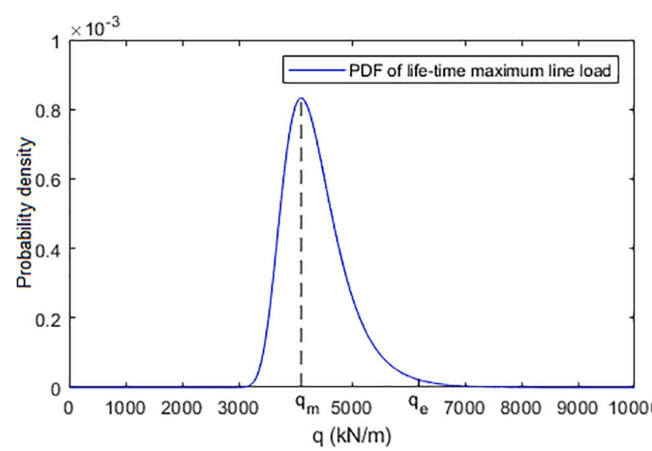

Fig. 21. PDF of the estimated life-time extreme line load.

taken into accounted with the extended EMM, which improves the generalization capability of the results.

We have demonstrated two estimation methods, one with maximum likelihood and the other with probability paper. The resulting model parameters differ slightly as the results of different estimation methods, but the estimations on extreme values are similar. One can adopt either resulting model for the estimation of extreme loads. The uncertainty analysis shows that the uncertainty in characteristic extreme value due to uncertainty in model parameters is relatively low. The predictive extreme distribution is rather similar to the extreme distribution based on point estimation using maximum likelihood, which indicates that for practical reason, point-estimation results can be used to define extreme loads.

7.2. Hidden factors

Although this paper has successfully taken concentration into account as the second ice condition variable, there are apparently other factors influencing the ice load distributions, e.g. floe size. One may expect a model relating β and x_0 to more influencing variables. Since the concept has been based on categorization of data, including more variables leads to higher dimensions and thus the number of categories significantly increases. This significantly increases the demand of data, but is worthwhile to investigate if the size of data is large enough.

Another hidden factor influencing the load magnitude is crew operation. One may drive the ship aggressively without voluntary speed reduction and collision avoidance, or cautiously by reducing speed and avoiding major collisions with ice floe. This apparently has an effect on the resulting load magnitude. The choice of ship crew is naturally affected by the ice condition which they observe. We could write the following relationships conceptually:

$$P(load|icecondition) = P(crewoperation|icecondition)*P(load|crewoperation, icecondition)$$

This paper has implicitly assumed that the underlying distribution of $P(crewoperation|icecondition)$ is unchanged among all the events, so that the distribution of ice load can be modeled only with ice conditions. In other words, the way ship crew operates the ship in response to the ice condition remains constant. The mode of crew operation naturally varies for different ships and crew. It is beneficial to quantify this through e.g. navigational data so that its influence on ice load can be taken into account.

7.3. Pathway towards a more generalized model

The results of this paper are obtained based on the measurement onboard S.A. Agulhas II. The validation with six-year data has demonstrated that the method is valid for the estimation of long-term extreme loads on the same frame of the same ship. Nonetheless, it does not tell whether such results can still give correct estimations for another ship with different hull form, e.g. different frame angles. The demonstration presented in Section 6 is based on the assumption that the imaginary ship has similar hull form as S.A. Agulhas II, so that the β and x_0 formulae can be applied without modification. However, if the frame angle differs considerably, it is then questionable whether the results remain valid. This is a typical difficulty with applying probabilistic models obtained from the measurement of one ship to different ships.

Another limitation still associated with the extended EMM is related to the definition of exposure. The results in this paper is based on ten-minutes maxima due to practical reasons. To apply the results, the exposure then needs to be defined based on the operation time in each ice condition category. For a fixed distance, the operation time is apparently linked to operation speed. Therefore, the results are based on the operation speed profile of S.A. Agulhas II. For a ship with different operation speed profile, the exposure then differs even if the ship goes on the same route as S.A. Agulhas II.

It is worthwhile to consider solutions which helps to generalize the probabilistic model obtained through the analysis of one ship to other ships. This is in principle possible. To account for the frame angles, corrections can be made on the calculated β and x_0 using physical knowledge on ship-ice interaction, similar to the attempt by Kujala [3]. To account for different operational profile, the ten-minute-maxima-based results derived in this paper can be converted to distance-based results using the operation profile of S.A. Agulhas II, which is then independent of operation profile thus suitable to be used for any other ships. These will improve the capability to generalize the results to other ships. This paper focused on the statistical modelling of ice loads on the measurement ship, while the solution of generalization is left to future work.

7.4. Other limitations and future work

The work in this paper is based on visually observed ice conditions, which contains relatively large uncertainty [25]. This leads to uncertainty in the obtained model and also leads to yearly variation if the model is established on a different training dataset as shown in Section 5.4. If the same method can be applied to data with more accurately measured ice conditions, the resulting model can be more reliable. With S.A. Agulhas II measurement, accurate ice condition monitoring has been made possible since 2018/19, when camera systems were instrumented on the ship to enable machine vision for concentration monitoring. In future when several years' measurement with accurate ice condition monitoring are obtained, it is worthwhile to carry out similar work to establish a new model and validate with long-term measurement. Another possible work to carry out is to include floe size as another ice condition variable, by which the ice condition characterization can be similar to the egg code of WMO [26]. The same principles can be followed as this paper, but one needs to carefully select the proper function form to model β and x_0 to include floe size as another variable. Once ice condition can be adequately characterized in the model, it becomes beneficial to consider the effect of ship speed and maneuvering (e.g. change of rudder angle) to the ice load magnitude.

8. Summary

This paper presents a probabilistic method for the analysis and long-term estimation of line loads on ship hull. The extension contains the modelling of x_0 and the inclusion of ice concentration as an additional ice condition parameter. Two different estimation methods were employed to establish the distribution parameter functions. Comparison of the results with the six-year measurement indicates that the proposed method provides good general agreement with data and is suitable for long-term estimation of ice loads.

Declaration of Competing Interest

The authors declare that they have no known competing financial interests or personal relationships that could have appeared to influence the work reported in this paper.

Acknowledgement

This project has received funding from the Lloyd's Register Foundation, a charitable foundation, helping to protect life and property by supporting engineering-related education, public engagement and the application of research www.lrfoundation.org.uk.

References

[1] Idrissova S, Bergström M, Hirdaris SE, Kujala P. Analysis of a collision-energy-based method for the prediction of ice loading on ships. Appl Sci 2019;9(21):4546.
[2] Sazidy M. Development of Velocity Dependent Ice Flexural Failure Model and Application to Safe Speed. Doctor thesis. Memorial University of Newfoundland; 2015.
[3] Kujala P. Semi-empirical evaluation of long term ice loads on a ship hull. Mar Struct 1996;9(9):849–71.
[4] Kotilainen M, Vanhatalo J, Suominen M, Kujala P. Predicting ice-induced load amplitudes on ship bow conditional on ice thickness and ship speed in the Baltic Sea. Cold Reg Sci Technol 2017;135:116–26.
[5] Suyuthi A, Leira BJ, Riska K. Statistics of local ice load peaks on ship hulls. Struct Saf 2013;40:1–10.
[6] Suominen M, Kujala P. Variation in short-term ice-induced load amplitudes on a ship's hull and related probability distributions. Cold Reg Sci Technol 2014;106-107:131–40.
[7] Chai W, Leira BJ, Naess A. Probabilistic methods for estimation of the extreme value statistics of ship ice loads. Cold Reg Sci Technol 2018;146:87–97.

[8] Shamaei F, Bergström M, Li F, Kujala P, Taylor R. Analysis and development of a probabilistic method for calculating local peak ice pressures on ships. Mar Struct 2020;74.
[9] Jordaan IJ, Maes M, Brown PW, Hermans IP. Probabilistic analysis of local ice pressures. J Offshore Mech Arct Eng 1993;115:83–9.
[10] Taylor RS, Jordaan IJ, Li C, Sudom D. Local design pressures for structures in ice: Analysis of full-scale data. J Offshore Mech Arct Eng 2010;132:1–7.
[11] Li C, Jordaan IJ, Taylor RS. Estimation of local ice pressure using up-crossing rate. J Offshore Mech Arct Eng 2010;132:1–6.
[12] Brown PW, Jordaan IJ, Nessim MA, Haddara MMR. Optimization of bow plating for icebreakers. J Sh Res 1996;40:70–8.
[13] Ralph F. Design of ships and offshore structures: a probabilistic approach for multi-year ice and iceberg impact loads for decision-making with uncertainty. Doctor thesis. Memorial University of Newfoundland; 2016.
[14] Rahman MS, Taylor RS, Kennedy A, Ré AS, Veitch B. Probabilistic analysis of local ice loads on a lifeboat measured in full-scale field trials. J Offshore Mech Arct Eng 2015;137:1–14.
[15] ISO 19906. Petroleum and natural gas industries — Arctic offshore structures 2019.
[16] Suominen M, Romanoff J, Remes H, Kujala P. The determination of ice-induced loads on the ship hull from shear strain measurements. Anal Des Mar Struct V 2015:375–83.
[17] Suominen M, Aalto H, Kulovesi J, Lensu M, Kujala P, Soal K, et al. In: Ship-based visual Antarctic sea ice thickness measurements. Michigan USA: Ann Arbor; 2016. p. 1–8.
[18] Suominen M, Bekker A, Kujala P, Soal K, Lensu M. Visual Antarctic sea ice condition observations during austral summers 2012–2016. POAC: Proc. Int. Conf. Port Ocean Eng. under Arct. Cond; 2017.
[19] Sandru A, Hyyti H, Visala A, Kujala P. A complete process for shipborne sea-ice field analysis using machine vision. Int. Fed. Autom. Control World Congr., Berlin, Germany: 2020.
[20] Kujala P, Jiang Z, Li F, Lu L. Long term prediction of local ice loads on the hull of S. A. Agulhas II. Proc 25th Int Conf Port Ocean Eng under Arct Cond Delft. Netherl 2019.
[21] Lu L, Kujala P. Full-Scale Measurements on board S.A. Agulhas II during SANAP 2018/2019 and Weddell Sea Expedition 2019. 2019.
[22] Lu L, Kujala P, Banda OAV, Goerlandt F. Ramming induced ice loads between the ship bow and multiyear thick ice in antarctic weddell sea. Dev. Collis. Grounding Ships Offshore Struct. - Proc. 8th Int. Conf. Collis. Grounding Ships Offshore Struct. 2020.
[23] Sanderson T, Cold S, Engineering R. Ice Mechanics and Risks to Offshore Structures 1987.
[24] Bergström M, Erikstad SO, Ehlers S. Assessment of the applicability of goal- and risk-based design on Arctic sea transport systems. Ocean Eng 2016;128:183–98.
[25] Suominen M, Kulovesi J, Lensu M, Lehtiranta J, Kujala P. A Comparison of Shipborne Methods for Ice Thickness Determination. Proc. 22nd IAHR Int. Symp. Ice, 2014.
[26] WMO. Sea Ice Nomenclature. vol. 1. 2014.